POLYPUBLIE
Polytechnique Montréal

POLYTECHNIQUE MONTRÉAL
UNIVERSITÉ D'INGÉNIERIE

Titre: Title:	Doping of silicon studied by X-ray photoemission spectroscopy
Auteur: Author:	Zheng-Hong Lu
Date:	1989
Type:	Mémoire ou thèse / Dissertation or Thesis
Référence: Citation:	Lu, Z.-H. (1989). Doping of silicon studied by X-ray photoemission spectroscopy [Ph.D. thesis, Polytechnique Montréal]. PolyPublie. https://publications.polymtl.ca/57958/

Document en libre accès dans PolyPublie
Open Access document in PolyPublie

URL de PolyPublie: PolyPublie URL:	https://publications.polymtl.ca/57958/
Directeurs de recherche: Advisors:	
Programme: Program:	Unspecified

Ce fichier a été téléchargé à partir de PolyPublie, le dépôt institutionnel de Polytechnique Montréal
This file has been downloaded from PolyPublie, the institutional repository of Polytechnique Montréal

https://publications.polymtl.ca

UNIVERSITE DE MONTREAL

Doping of Silicon Studied by X-Ray Photoemission Spectroscopy

par

Zheng-Hong Lu
DEPARTEMENT DE GENIE PHYSIQUE
ECOLE POLYTECHNIQUE

THESE PRESENTEE EN VUE DE L'OBTENTION
DU GRADE DE PHILOSOPHIAE DOCTOR (Ph.D.)
(GENIE PHYSIQUE)

May 1989

© Zheng-Hong Lu, 1989

National Library of Canada

Bibliothèque nationale du Canada

Canadian Theses Service

Service des thèses canadiennes

Ottawa, Canada
K1A 0N4

The author has granted an irrevocable non-exclusive licence allowing the National Library of Canada to reproduce, loan, distribute or sell copies of his/her thesis by any means and in any form or format, making this thesis available to interested persons.

The author retains ownership of the copyright in his/her thesis. Neither the thesis nor substantial extracts from it may be printed or otherwise reproduced without his/her permission.

L'auteur a accordé une licence irrévocable et non exclusive permettant à la Bibliothèque nationale du Canada de reproduire, prêter, distribuer ou vendre des copies de sa thèse de quelque manière et sous quelque forme que ce soit pour mettre des exemplaires de cette thèse à la disposition des personnes intéressées.

L'auteur conserve la propriété du droit d'auteur qui protège sa thèse. Ni la thèse ni des extraits substantiels de celle-ci ne doivent être imprimés ou autrement reproduits sans son autorisation.

ISBN 0-315-58211-1

Canada

UNIVERSITE DE MONTREAL

ECOLE POLYTECHNIQUE

cette thèse intitulée:

Doping of Silicon Studied by X-Ray Photoemission Spectroscopy

présentée par : Zheng-Hong Lu

en vue de l'obtention du grade de: Philosophiae Doctor

a été dûment acceptée par le jury d'examen constitué de:

Mr. J.F. Currie ...., Ph.D., président

Mr. J.L. Brebner ...., Ph.D.

Mr. P.R. Norton ...., Ph.D.

Mr. A. Yelon ...., Ph.D.

Abstract

Highly degenerate Ga-doped amorphous and crystalline silicon have been prepared using 4 KeV liquid metal ion gun implantation and rapid thermal anneal, and studied using x-ray photoelectron spectroscopy (XPS) and low energy electron diffraction (LEED).

Photoemission valence-band density-of-states (VB-DOS) and LEED measurements show that the crystalline silicon lattice is amorphized by Ga^+ ions at a dose of 15 at.%. Amorphous silicon structural relaxation is observed on low temperature (≤ 400 ^oC) annealed samples. Annealing at, or above 500 ^oC, is found necessary for a complete solid-phase epitaxial regrowth of the damaged layer.

Ga 3d core level studies indicate that the chemical nature of the majority of as-implanted gallium is in the elemental state (Ga^o), along with a very small amount of two-fold coordinated Ga (Ga^2) bonded to the damaged silicon lattice. The Ga^2 is an unstable configuration in the amorphous silicon lattice, and disappears after annealing. The low temperature ($\leq 400^oC$) activated Ga is found to ocupy either a 3-fold sp^2 or a 4-fold sp^3 hybrid. The heat, H_{SR}, released by Si lattice structural relaxation or bond-angle ordering, is shown to be the prime energy source for dopant activation in this temperature regime. The fraction of substitutional Ga or doping efficiency in amorphous silicon (a-Si) is found to be closely related to the a-Si continuous-random-network (CRN) bond-angle distribution function $P(\theta)$, ranging from 5 to 10 % at dopant levels around 10 at.%. A $P(\theta)$ controlled dopant-defect auto-compensation doping mechanism of the amorphous silicon is proposed. This model predicts that the doping efficiency has a square-root relation with total dopant concentration at low doping level, and a constant value at high doping level. A maximum doping efficiency of 10 % is suggested as due to the

fact that there is a minimum width of P(θ) maintaining a stable a-Si CRN prior to crystallization.

Si 2p core electron measurements provide us the most direct experimental evidence of annealing-promoted tetrahedral Si-Ga bonds. The Ga, as high as 10 at.% after an anneal at 500 ^oC, was found to occupy substitutional sites close to the surface. The surface concentration decreased with increasing annealing temperature. We show that supersaturated Si-Ga bonds can induce an energy shift of the valence band maximum (VBM) toward the vacuum level.

We found the full width at half maximum (FWHM) of Si 2p core levels decreasing with increasing annealing temperature. A large FWHM on low temperature ($\leq 400^o$) annealed samples is explained as due to Si-Si bond-length and bond-angle variation-induced static charge fluctuations Δq_{rms} in the unreconstructed a-Si CRN. The broad FWHM on samples with well reconstructed lattices on anneal $\geq 500^oC$. however, is interpreted as due to strains induced by the Si-Ga bonds . The static charge fluctuations Δq_{rms} is estimated at 0.11 electrons in amorphous silicon. In degenerate c-Si samples, Δq_{rms} varies from 0.04 to 0.003 electrons, depending upon the Si-Ga density.

Sommaire

En technologie de micro-électroniques à très haut degré d'intégration de type "CMOS", en particulier leur haute densité et haute vitesse nécessitent des jonctions étroites et très conductrices. La fabrication de jonctions p-n étroites par implantation ionique de B à faible énergie est difficilement réalisable à cause du phénomène de canalisation. Le Ga est un des accepteurs du Si. Puisque la masse atomique du Ga est six fois plus grande que celle du B, la profondeur de pénétration des ions des Ga est plus petite que celle des ions de B et la canalisation des ions de Ga aussi réduite de facon significative parce que une couche amorphe est plus facilement produite avec une densité de 10^{14} cm^{-2}. La couche amorphe peut être recristallisé par recuit rapide à une température de 500 - 600 ^{0}C. Cette couche sera très active, la concentration de porteurs libres pourra dépasser la solubilité maximum en phase solide du Ga dans le Si.

Il est évident que l'étude des procedés d'activation des dopants et de la recristallisation épitaxiale au Si implanté ioniquement est importante pour la comprehension des propriétés physico-chimiques des dopants dans le Si amorphe ou cristallin, et ainsi que pour des applications techniques. La rétrodiffusion de Rutherford, la canalisation et la microscopie électronique par transmission (MET) ont été les principales techniques analytiques utilisées pour étudier l'implantation ionique depuis quelques décennies. Cependant, la rétrodiffusion de Rutherford et le MET sont insensibles à l'environnement chimique local et particulièrement pour les échantillons dont le réseau perturbé n'a pas été complètement reconstruit. La spectroscopie par photoémission, une technique analytique bien développée, est sensible à ces points. Le princible de base de cette technique est que les électron, excités par des photons, provenant des orbitale électroniques prés du noyau ou de valence sont analysés par rapport à l'énergie des photons. Ainsi, la densité d'états

des bandes de valence déterminée par photoémission est une description de la distribution électronique de la couche de valence, laquelle est reliée à l'arrangement atomique local du Si. Les niveaux électroniques près du noyau sont sensibles aux différentes configurations de liaisons chimiques. Donc la spectroscopie par photoémission procure une opportunité unique de sonder les différentes configurations du Ga implanté dans le Si après différentes étapes de recuit, et de connaître la relation entre le nombre de Ga différemment lié et l'arrangement local du Si.

Dans cette thèse, le silicium amorphe et cristallin dopé au Ga ont été, préparé en employant l'implantation par canon ionique à métal liquide ainsi que le recuit thermique rapide, et étudié en utilisant la spectroscopie photoélectronique ainsi que la diffraction des électrons lents (LEED).

La mesure de la densité d'états de la bande de valence par photoémission (VB-DOS) et par la technique LEED montre que le réseau de silicium est rendu amorphe par les ions Ga^+ à une concentration de 15 at.%. La relaxation structurelle du silicium est observée sur des échantillons recuits à basse température ($\leq$ 400 °C). Un recuit à 500 °C est cependant nécessaire pour retourer la cristallineté de la couche endommagée par épitaxie en phase solide.

Des études du niveau profond 3d dans le Ga montrent que la majeure partie du gallium implanté par la méthode décrite plus haut a une nature chimique élémentaire (Ga^o), alors qu'une toute petite quantité de Ga ayant une coordination double (Ga^2) est liée au réseau endommagé du silicium. Le Ga^2 est une configuration instable dans le réseau de silicium, et disparait après recuit. On a montré que le Ga activé à basse température ($\leq$ 400 °C) occupe soit un hybride triple sp^2 ou quadruple sp^3. Il est également montré que la chaleur H_{SR} dégagée par la relaxation structurelle ou par réagencement angulaire dans le Si est une source d'énergie déterminante pour l'activation dans ce régime de température. On a trouvé que la fraction de Ga de substitution, ou, autrement dit, l'efficacité de dopage dans le silicium amorphe (a-Si) est étroitement liée à la distribution

angulaire P(θ) des liens (allant de 5 à 10 % pour une concentration de dopant de 10 at.%) du réseau-aléatoire-continu (CRN) du a-Si.

Nous avons trouvé que la densité d'états électronique de la bande de valence et modifiée par la prèsence des atomes de Ga. La densité d'états suplémentaire observée autour de 10 eV est interprètée comme une contribution des deux électrons de valence 4s des atomes de Ga inactifs. L'augmentation de la température du récuit, entraine l'augmentation des nombre d'atomes de Ga hybrides avec Si, par consequent la densité d'états, dans la région d'énergie 10 eV décroît.

Un mécanisme de dopage par auto-compensation des défauts induits par les dopants avec P(θ) contrôlé est proposé. Ce modèle prédit que l'efficacité de dopage évolue comme la racine carrée de la concentration totale de dopant à faible concentration et sature à forte concentration. Une efficaté maximale de dopage de 10% est prévue et cela parce qu'il existe une largeur minimum de P(θ) permettant d'avoir un CRN de a-Si stable avant cristallisation.

La mesure des électrons du niveau profond 2p dans le Si fournit la confirmation expérimentale la plus probante de l'existence de liens tétrahédraux Si-Ga générés par le recuit. On a trouvé que le Ga, atteignant 10 at.% après recuit, occupe des sites de substitution près de la surface. La concentration à la surface décroît avec l'augmentation de la température de recuit. Nous montrons que les liens Si-Ga supersaturés peuvent induire un déplacement du maximum de la bande de valence (VBM) vers sa position dans le vide.

Nous trouvons que la largeur à mi-hauteur (FWHM) du niveau 2p dans le Si décroît avec une augmentation de la température de recuit. Une grande valeur de la largeur à mi-hauteur pour des échantillons recuits à basse température ($\leq$ 400°) est attribuée à des fluctuations de la charge statique Δq_{rms} induite par des variations dans la longueur et l'angle des liens Si-Si dans le CRN reconstruit du a-Si. Par contre la grande largeur à mi-hauteur dans des échantillons ayant un réseau bien reconstruit par un recuit à des températures $\geq$ 500 °C est interprétée comme

étant due aux contraintes induites par les liens Si-Ga. Les fluctuations de la charge statique Δq_{rms} sont estimées à 0.11 électrons dans le silicium amorphe. Dans des échantillons c-Si dégénérés, Δq_{rms} varie de 0.04 à 0.003 électrons, dépendamment de la densité des liens Si-Ga.

Acknowlegments

It is a great pleasure that I have had the chance to complete my Ph.D. education under the the guidance of Drs. A. Yelon and E. Sacher, whose broad and in-depth understandings of science have illuminated me over copious perplexed crossings on my pursuit of the scientific true essence.

I owe an enormous debt of gratitute to Dr. and Mrs. G. Warfield, with whom many genuinely beneficial chats on numerous subjects are sincerely regarded and whose influence has been incalculable.

I would like to thank Dr. A. Okoniewski for kindly preparing the intrinsic a-Si:H, Dr. T. Catalano of the Solarex Corp. for providing the degenerate n^+ and p^+ a-Si:H samples, Ms. S. Poulin-Dandurand for assistance with the VG ESCALAB Mk II instrument manupulation, and Mr. Y.M. Huai for technical assistance in typing the manuscript.

During the course of studies, assistance from other GCM members were received and appreciated: Dr. A. Azelmad, Dr. J. Brebner, Mr. A. Cambron, Dr. R.W. Cochrane, Dr. J.F. Currie, Mr. B. Malo, Mr. M. Kemp, Ms. J. Klemberg-Sapieha, Mr. C. Lagarde, Ms. C. Morin, Dr. C. Tannous, and Dr. A. Selmani.

This work was supported by CRSNG and Fonds FCAR.

Zheng-Hong Lu

Montreal, June 1989

Contents

Abstract iv

Sommaire iv

Acknowlegments x

List of Tables xiii

List of Figures xiv

1 INTRODUCTION 1

2 X-Ray Photoelectron Spectroscopy 7

2.1 The Basics of X-Ray Photoelectron Spectroscopy 7

2.2 Elemental Analysis 13

2.3 Core Level Chemical Shift 13

2.4 The Spin-Orbit Interaction and Nomenclature 16

3 EXPERIMENTAL 20

3.1 Si Surface Preparation And Characterization 20

3.2 Implantation of Ga in Silicon 26

3.3 Rapid Thermal Annealing 28

3.4 X-Ray Photoelectron Spectroscopy 32

4 RESULTS AND DISCUSSION 38

4.1 Structural Relaxation and Crystallization of Amorphous Silicon Studied by Photoemission VB Spectroscopy 38

4.2 VB-DOS Variation with Ga Atomic Orbital Hybridization 44

4.3 Ga Coordination Numbers in Amorphous Silicon Determined by Core Level Photoemission Spectra 49

4.4 Activation of Ion-Implanted Ga Atoms and Doping Efficiency of Amorphous Silicon 55

4.5 Amorphous Silicon Doping Mechanism 59

4.6 Supersaturated Substitutional Ga in Crystalline Silicon Studied by Si 2p Core Level Spectra 67

4.7 Static Charge Fluctuations in Si 74

5 CONCLUSION 78

BIBLIOGRAPHY 81

List of Tables

2.1 X-ray and spectroscopic notation. 17

2.2 Spin-orbit coupling energy. 18

2.3 Spin-orbit splitting parameters. 19

4.1 ΔE_{3p} as a function of annealing temperatures. 45

4.2 Hartree-Fock s- and p-orbital energy. 48

4.3 Fractions of differently coordinated Ga. 56

4.4 Elemental electronegativities of nontransition atoms in tetrahedrally coordinated enviroments. 63

4.5 XPS data for Ga-implanted c-Si. 73

4.6 Calculated static charge fluctuations in Si. 77

List of Figures

1.1	Computer-generated pictures of silicon.	4
2.1	Schematic representation of the photoemission.	8
2.2	Mean free path of electrons in solids.	9
2.3	Calculated cross-sections.	11
2.4	Schematic representation of the photoemission process and energy levels involved.	12
2.5	Electron spectrum from carbon ethyl trifluroacetate.	15
3.1	A typical LEED pattern observed from a Si(111) surface.	24
3.2	Si2p core level spectra.	25
3.3	Illustration of the determination of the sputter-rate by the masking technique.	29
3.4	The distribution of ion-implanted Ga in Si measured by XPS and Ar ion sputtering.	30
3.5	Calculated Ga profiles at different energies.	31
3.6	Illustration of the VG ESCALAB MK II instrument.	33
3.7	Illustration of the electron energy analyser.	34
3.8	Nickel valence photoelectron EDC.	36
3.9	Photoemission valence band density of states of Si.	37

4.1 Experimental VB-DOS of c-Si and a-Si:H. 39
4.2 VB-DOS of Ga implanted and annealed a-Si:H. 42
4.3 VB-DOS of Ga implanted and annealed c-Si. 43
4.4 VB-DOS of a-Si:H and c-Si modified by Ga. 47
4.5 Ga3d core level spectra measured on c-Si substrates. ... 51
4.6 Electronegativities of carbon, nitrogen and oxygen as a function of percent s character. 53
4.7 Ga3d core level spectra measured on a-Si:H substrates. .. 54
4.8 Variations of three and four fold coordinated Ga. 57
4.9 A two dimensional a-Si growth model. 62
4.10 Doping efficiency as a function of concentration. 66
4.11 Si2p core level spectra. 68
4.12 A two dimentional model of four possible Ga-in-Si configurations. 70
4.13 Arrhenius plot of the substitutional Ga and annealing temperature. 71

Chapter 1

Introduction

In large scale integration technology, especially for complementary metal-oxide-semiconductor (CMOS) integrated circuits, highly conductive shallow junctions are required for small device fabrication in order to achieve higher packing density and faster switching speed. The fabrication of shallow p^+-n junctions by low energy B^+ ion implantation is found impractical due to the channelling effect (Michel et al 1984). Ga is one of the acceptors in Si. Since the mass of Ga is six times larger than that of B , the projected range of Ga^+ ions is shorter than that of B^+ ions and the channeling by Ga^+ ions is also significantly reduced because an amorphous layer is more easily produced at a dose of 10^{14} cm^{-2}. The amorphous layer can be solid-phase epitaxially (SPE) regrown by transient rapid thermal annealing (RTA) in a low-temperature regime of 500–600 °C, resulting in a highly activated thin layer in which free-carrier concentration exceeds the maximum solid solubility of Ga in Si (Matsuo et al. 1987, Harrison et al. 1987, Lin et al. 1988, Lu et al. 1989a).

It is obvious that studying the dopant activation process and SPE regrowth of ion-implanted silicon is important for the understanding of the chemico-physical properties of the dopant in either amorphous or crystalline silicon, and as well as for the technical applications. Rutherford back-scattering (RBS), channelling

and transmission electron microscope (TEM) have been the major analytical techniques used to study ion implantations in the past few decades. However, both RBS and TEM are insensitive to the local chemical enviroments and valence electron states of Si and of the implant, especially for samples in which the damaged lattice has not been completely reconstructed. Photoemission spectroscopy, a well developed analytical technique, is sensitive to these. The basic principle of this technique is that photon-excited electrons from elemental core and valence orbitals are analyzed with respect to the the photoelectron energy. Thus the photoemission valence band density of state (PVB-DOS) is a direct description of the valence shell charge distribution, which in turn is correlated with the local Si atomic arrangement. The elemental core level is also sensitive to the valence shell charge distribution which is different for various chemical bond configurations. Therefore photoemission spectroscopy provides a unique opportunity to probe the ion-implanted Ga configurations in Si at various stages of post-annealing, and the relation between the number of differently bonded Ga and local host Si atom topological arrangements.

Surprisingly little work has been done in this area. Although several research groups have used photoemission spectroscopy to study As^+ ion-implanted silicon surface properties (Eastman et al. 1981) and Si^+ ion-implanted silicon bulk structures (Vasquez et al. 1985), there is no systematic and comprehensive research work reported. In terms of probing the chemical nature of ion-implanted materials, we have found very little work done in this field(Lu et al. 1989a,c).

The structure of crystalline silicon is diamond-cubic. In a continuous diamond-cubic network of crystalline silicon, Si atoms are bonded to each other through covalent bonding, with the same bond-length of 2.35 Å, and the same bond-angle of 109.5^0. In Fig.1.1a, we show the computer simulated c-Si continous network(Winer 1987). In non-crystalline or amorphous(a-) Si network, there is a significant spread in the bond-length and bond-angle; typically bond-angle distortions are found to

be about 10%. and bond-length distortions are 1% or less(Elliott 1983). In Fig.1.1b, we show the computer simulated a-Si continuous network(Winer 1987). As a-Si continuous network does not possess long-range order, it is often referred to as a-Si continuous random network (CRN). It has been found that there are dangling bonds (threefold-coordinated Si atoms) in the a-Si CRN. As Si dangling bonds produce energy states in the middle of the energy gap. they can trap the conduction electrons. This is bad for most of the applications of a-Si in making electronic devices. The bonding and anti-bonding energy states of Si-H bond are found either below the valence band maximum (Si-H bonding) or above the conduction band minimum (Si-H anti-bonding)(Ley 1984a). Therefore, Si-H bond can efficiently passivate the Si dangling bonds. This makes the amorphous silicon a more attractive electronic material in terms of application. The a-Si CRN contained Si-H bonds is called hydrogenated amorphous silicon (a-Si:H) to distinguish from pure amorphous silicon (a-Si).

The dopant coordination numbers in amorphous semiconductor have been long a disputed subject. In 1967 Mott introduced the "8-N" (N is the number of valence electrons) rule to account for the "absence" of doping in covalent amorphous semiconductors. The suggestion was that element coordinations in an amorphous network satisfy their valence requirements locally in the absence of constraints due to periodicity: electrons are paired and the bond number n_c obeys the "8-N" rules, viz n_c = 8-N for N>4 and n_c =N for N<4. Thus the coordination number of Si is 4. of Ga is 3. etc.. This rule works extremely well for amorphous chalcogenides, for example. Thus these materials are virtually impossible to dope. When in 1975 Spear and LeComber showed that hydrogenated amorphous silicon (a-Si:H) could be substitutionally doped by the addition of small amounts of phosphine and diborane to the silane plasma. this discovery came as a surprise to many workers in the field. and thereafter activated extensive research that significantly improved our understanding of this material (Pankove 1984). Tech-

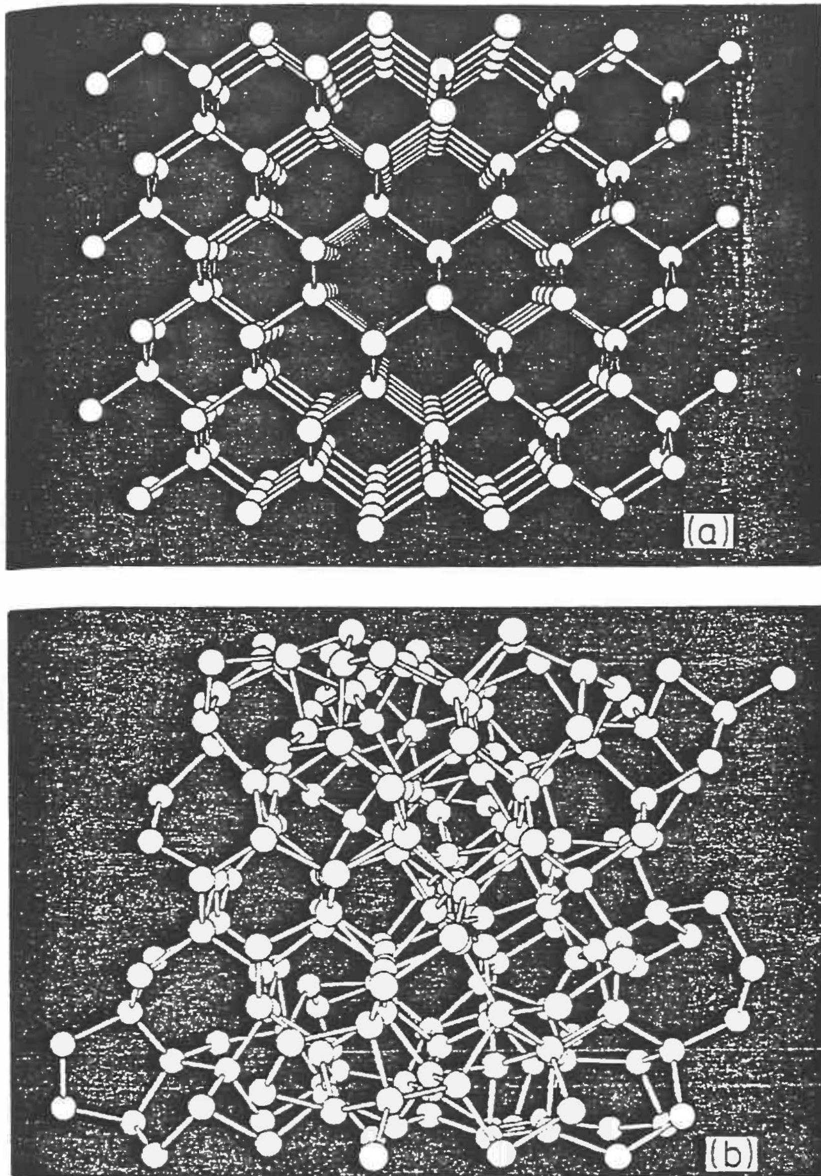

Figure 1.1: Computer-generated pictures of (a) diamond-structure silicon and (b) the CRN silicon. Viewed toward the (110) face.

nologically, various a-Si:H-based thin film electronic devices, especially solar cells have been developed, and now commercialized (Pankove 1984). Different experimental techniques such as extended x-ray-absorption-fine-structure (EXAFS) and nuclear magnetic resonance (NMR) have been used to probe the chemical bonding of dopants in a-Si:H. Measurements on As and P in a-Si:H suggested a fraction of 4-fold coordinated donors as high as 20% for samples with total concentrations around 1 at.% (Knights et al 1977, Reimer and Duncan 1983). Based on electrical measurements, however, Stutzmann (1986) and Jousse et al (1987) showed that the solid-phase doping efficiency is less than 10% for various dopants over a wide range of doping levels. X-ray photoelectron spectroscopy (XPS) was also used to identify the chemical structures of boron in glow discharge (GD) deposited a-Si:H (Kazahaya and Hirose 1986). The two B 1s peaks deconvoluted were interpreted as trigonal sp^2 and tetrahedral sp^3 boron bonded to the amorphous silicon random network.

The object of this thesis is to use a liquid metal ion gun (LMIG) to introduce Ga atoms into both c-Si (the lattice is amorphised by Ga^+ ions and therefore become a-Si) and a-Si:H substrate close to the surface by ion implantation at low energy (4 keV). The implanted samples are post-annealed at various temperatures using RTA technique. XPS and low energy electron diffraction (LEED) are used to:

(1) study the Ga configurations in the amorphous silicon random network, the relation between the number of differently bonded Ga and local Si atom topological arrangements, the solid-phase doping efficiency of Ga in a-Si and the doping mechanism of amorphous semiconductors.

(2) analyse the Ga activation and the damaged Si lattice reconstruction process, and their corresponding thermodynamics.

(3) investigate the modifications to the Si valence band density of states by Ga^+ ions, Ga atoms, and Si-Ga bonds.

(4) measure the supersaturated substitutional Ga in c-Si which is obtained by LMIG ion-implantation and RTA annealing.

(5) determine the strains or static charge fluctuations in amorphous silicon brought about by Si-Si bond-angle and bond-length variations, and those in c-Si lattice induced by tetrahedral Si-Ga bonds.

Chapter 2

X-Ray Photoelectron Spectroscopy

2.1 The Basics of X-Ray Photoelectron Spectroscopy

Photoelectron spectroscopy is based on external photoelectric effect: The sample is irradiated with light of energy $h\nu$ and photoelectrons emitted from both core levels and valence shell are analysed with respect to their energy in an electrostatic energy analyzer equipped with electron detector and counting electronics (Fig 2.1). The measured quantity is the energy spectrum $I(E_k)$ of the photoelectrons, where E_k denotes the kinetic energy. It is advantageous and customary to introduce binding energies E_B through

$$E_B = h\nu - E_k - \Phi_A \tag{2.1}$$

where Φ_A is the sample work function, which is generally a few electron volts. The binding energies E_B are characteristic for a given material and do not depend on the photon energy hν as does E_k. The spectra so obtained can be interpreted

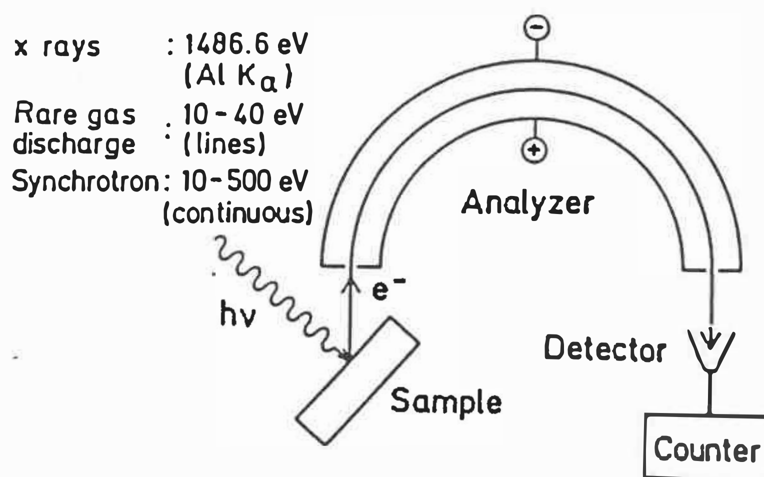

Figure 2.1: Schematic representation of the photoemission experiment.

using the three-step model first proposed by Spicer (1958). These steps are

(1) the excitation of the electron with absorption or annihilation of the photon.

(2) the transport of the excited electron through the solid to the surface.

(3) the escape of the electron from the confines of the solid into vacuum.

The energy distribution curve (EDC) of the photoemitted electrons $I(E_k)$ is consequently a sum of a primary distribution of electrons $I_p(E_k)$ that have not suffered an inelastic collision and a background of secondary electrons $I_s(E_k)$ due to electrons that have undergone one or more inelastic collisions.

$$I(E_k) = I_p(E_k) + I_s(E_k) \tag{2.2}$$

The primary distribution is factorized according to the three-step model into

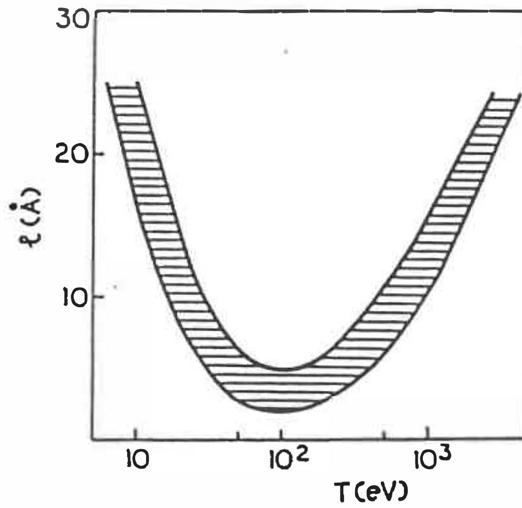

Figure 2.2: Kinetic energy dependence of the mean free path of electrons in solids. The shaded area corresponds to the region occupied by the actual experimental points for most materials (from Margaritondo and Weaver (1985)).

a distribution of photoexcited electrons $J(E_k, \omega)$, a transmission function $T(E_k)$, and an escape function $D(E_k)$.

$$I_p(E_k, \omega) = J(E_k, \omega) \cdot T(E_k) \cdot D(E_k) \tag{2.3}$$

where ω is the angular frequency of photon. Under the assumption that inelastic scattering probability can be characterized by an isotropic electron mean free path $\lambda_e(E_k)$, $T(E_k)$ is then given by

$$T(E_k) = \frac{\lambda_e(E_k)/\lambda_{ph}(\omega)}{1 + \lambda_e(E)/\lambda_{ph}(\omega)} \tag{2.4}$$

where $\lambda_{ph}(\omega)$ is the photon penetration depth which exceeds hundred Angstroms, and $\lambda_e(E_k)$ is the energy related electron mean free path as shown by the graph in Fig 2.2. For the most analyzed electrons with energies ($10 \leq E_k \leq 1000$ eV), λ_e is seen to vary between 4 Å to 20 Å so that $T(E_k)$ is < 0.05.

The short mean free path of the electrons effectively limits the sampling depth

of XPS to about 20 atomic layers. It should be kept in mind, however, that the genuine surface electronic structure extends no more than 2 to 3 atomic layers into the bulk so that EDCs will normally represent bulk properties (Appelbaum and Hamann 1976, 1978; Forstmann 1977).

The factor $D(E_k)$ takes into account the fact that photoelectrons have to overcome a surface barrier before they emerge into the vacuum. Both $D(E_k)$ and $T(E_k)$ are slowly-varying functions of E_k so that the $I_p(E_k, \omega)$ represents the structure of $J(E_k, \omega)$.

For electrons at the inner core levels, $J(E_k, \omega)$ or the spectral shape is – aside from energy analyzer contributions – given by a Lorentzian function with a width Γ determined by the lifetime τ of the hole left behind after photoexitation according to Heisenberg's uncertainty relation $\Gamma = \hbar/\tau$ (Cardona and Ley 1978).

For valence shell electrons, in the case of semiconductors, $J(E_k, \omega)$ is determined by (Ley 1984a)

$$J(E_k, \omega) \propto \mid P(\omega) \mid^2 \cdot N_v(E_k - h\omega) \cdot N_c(E_k) \tag{2.5}$$

where $P(\omega)$ is transition matrix element, (N_v, N_c) are valence and conduction band density of states. For the photon energies used in XPS, the final state electrons have wavelengths which are significantly short compared to interatomic distances. The matrix elements are therefore mainly determined by the rapidly varying segments of the initial state wave functions close to the atom core so that $J(E_k, \omega)$ is largely determined by the valence band density of states. From a quantum chemical point of view, we can divide $J(E_k, \omega)$ into each valence electron contribution, then (Ley 1984a)

$$J(E_k, \omega) \propto \sigma_s(\omega) \cdot N_s(E) + \sigma_p(\omega) \cdot N_p(E) \tag{2.6}$$

where $\sigma_{s,p}(\omega)$ and $N_{s,p}$ are the photoionization cross sections and partial densities of valence s and p atomic levels. The discussion considers elements which have s

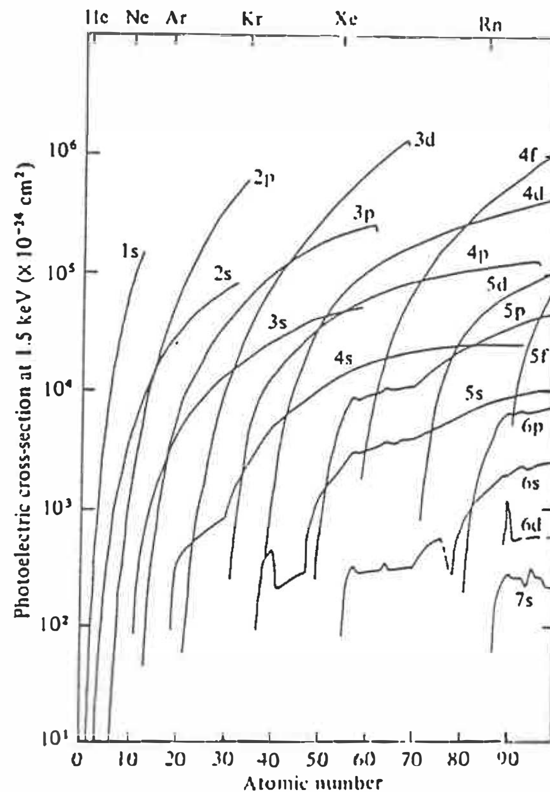

Figure 2.3: Calculated cross-sections for photoemission from occupied orbitals of elements for 1.5 keV photons (from Wertheim (1978)).

and p orbitals. The concept, however, is usable for other elements having d and f orbitals.

The calculated cross-sections for photoemission from occupied orbitals of the elements for 1.5 keV photons are given by graphs in in Fig. 2.3.

The above discussions are schematically summarized in the energy diagram of Fig. 2.4.

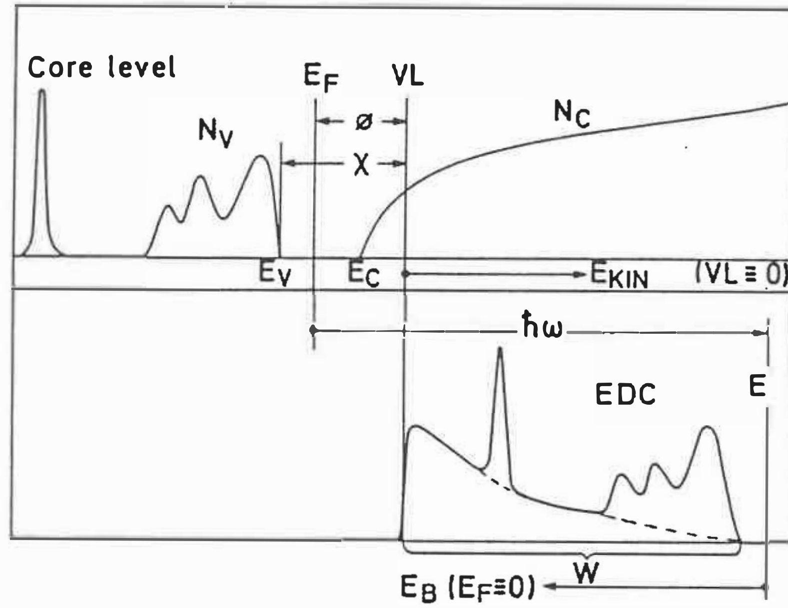

Figure 2.4: Schematic representation of the photoemission process and the energy levels involved.The upper half represents the level scheme of the semiconductor including one core level and the lower panel depicts the energy distribution of the photoelectrons (EDC). (N_v, N_c) valence and conduction band densities of states; (E_v, E_c) valence and conduction band edges; (χ) photoemission threshold; (ϕ) work function; (E_F) Fermi level; (VL) vacuum level; ($\hbar\omega$) photon energy; (W) width of EDC. The dashed line indicates the background of inelastically scattered electrons(from Ley (1984a)).

2.2 Elemental Analysis

The binding energies of core levels are characteristic of each element. Core level spectra are therefore used to identifiy the composition of specimens within the sampling depth of XPS. The intensity of a core level j from element Z, $I(j, Z)$, is related to the concentration $c(Z)$ of this element according to(Ley 1984a)

$$I(j, Z) = F \cdot \sigma(j, Z, \omega) \cdot c(Z) \cdot T(E) \cdot D(E) \cdot A(E) \tag{2.7}$$

where σ is the photoelectron cross section of the core level and $T(E)$ and $D(E)$ are the transmission and escape functions, respectively. $A(E)$ is the energy-dependent transmission function of the analyzer and F is an energy-independent scale factor that takes photon intensity and geometrical factors into account.

It is useful and customary to introduce an atomic sensivity factor, $s(j, z)$, through

$$s(j, z) = F \cdot \sigma(j, z, \omega) \cdot T(E) \cdot D(E) \cdot A(E) \tag{2.8}$$

Thus a general expression for the determination of the atom fraction of any constituent in a sample, $c(Z_x)$, can be written as

$$c(Z_x) = \frac{I(j, Z_x)/s(j, Z_x)}{\sum_i I(j, Z_i)/s(j, Z_i)} \tag{2.9}$$

$s(j, Z)$, based on either peak height or area, can be determined from well-defined compounds, and is listed in relevant books (Briggs and Seah 1983).

2.3 Core Level Chemical Shift

The principal application of x-ray photoelectron spectroscopy is to identify chemical enviroment and valence electron state of an element by comparison of its core-level binding energies with those of a set of reference compounds involving the same element. If we consider a core level, the energy of an electron in this state is determined by the attractive potential of the nuclei and the repulsive

Coulomb interaction with all of other electrons of the system. Any change in the chemical enviroment of the element will involve a spatial redistribution of the valence electron charges of this atom and the creation of a different potential as seen by a core electron. This charge redistribution will lead to a change in the core level electron binding energies.

A good illustration of the chemical structure dependence of binding energy in organic compound is seen in the spectrum of the carbon 1s levels in ethyl trifluoroacetate (Fig 2.5), recorded by Siegbahn and coworkers (1967). In this molecule there are four structurally distinguishable carbon atoms, corresponding to the four resolved lines that appear in the spectrum.

Experimentally, it is found that chemical shift ΔE_B of a core level is correlated to valence charge transfer Δq in the formation of chemical bonds according to (Ley 1984a)

$$\Delta E_B = \beta \cdot \Delta q \tag{2.10}$$

The proportional constant β takes a value of approximately -2.2 eV per electron for the 2p level of silicon, as derived from chemical shift data on SiO_x (Grunthaner et al 1979). The numerical value assigned to β obviously depends upon the way the valence electrons are divided among the partners participating in an ionic or partially ionic bond. The tendency of charge transfer can be determined using the chemical bond ionicity f_i derived by Pauling (1967). The ionicity f_i is expressed in terms of the difference in electronegativities X_A and X_B of the two participating atoms, according to

$$f_i = 1 - \exp\{-0.25(X_A - X_B)^2\} \tag{2.11}$$

The effective charge on atom x is $q_x = \gamma_x \cdot f_i$, where γ_x is the coordination number of atom x (Ley 1984a).

The concept of bond ionicity is often helpful in predicting the signs of chemical shifts. An atom with a larger electronegativity value than those of other participating atoms will attract more electrons to its valence shell, and thereby affect the

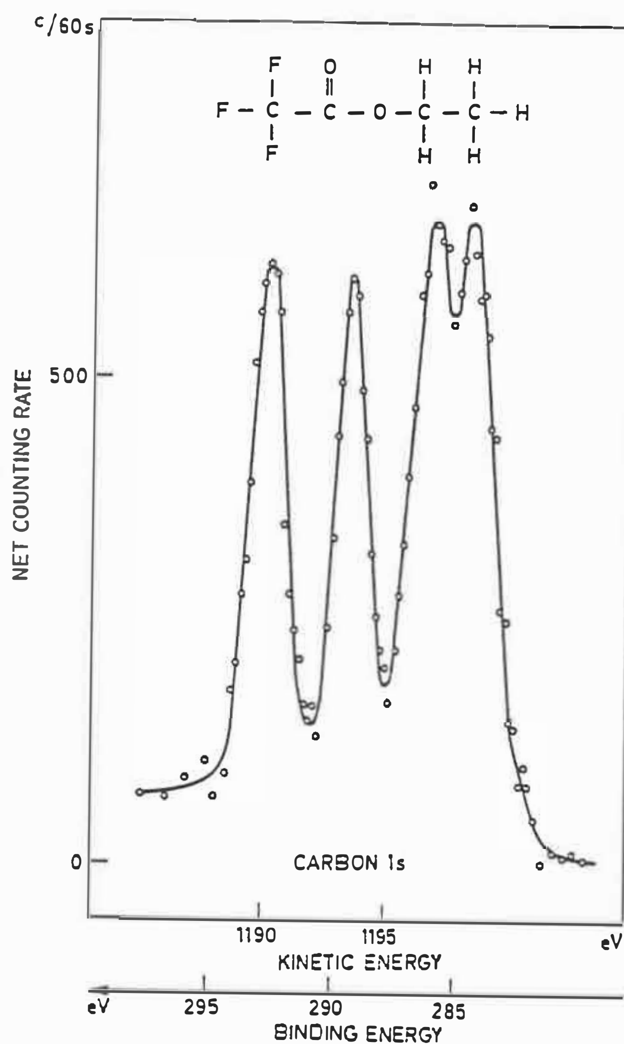

Figure 2.5: Electron spectrum from carbon in ethyl trifluroacetate. All four carbon atoms in this molecule are distinguishable in the spectrum. The lines appear in the same order from left to right as do the corresponding carbon atoms in the structure that has been drawn in the figure.

core levels by shifting the binding energies of the electron at these levels toward the vacuum level.

2.4 The Spin-Orbit Interaction and Nomenclature

Since electron is a charged particle, its orbit (with the characteristic quantum number $l, l = 0, 1, 2, 3, 4, \ldots$) around a nucleus will induce a magnetic field, which will interact with the electron's inherent magnetic field produced by the spin (with spin quantum number $s = \pm 1/2$). The interaction energy ΔE_j is given by (Chen 1985)

$$\Delta E_j = \frac{1}{m^2c^2} \cdot \frac{1}{r} \cdot \frac{dV(r)}{dr} \cdot (\vec{S} \cdot \vec{L}) \tag{2.12}$$

where m is the electron mass, c is the speed of light, r is the orbital radius, V(r) is the central force potential, and $\vec{S}$ and $\vec{L}$ are the spin and orbit vectors respectively.

If we introduce the total angular momentum through $\vec{J} = \vec{S} + \vec{L}$, then ΔE_j can be expressed as (Chen 1985)

$$\Delta E_j = \frac{1}{2m^2c^2} \cdot \frac{1}{r} \cdot \frac{dV(r)}{dr} \cdot [j(j+1) - l(l+1) - \frac{3}{4}] \tag{2.13}$$

Obviously, j can take the values $l \pm \frac{1}{2}$ for a given l number. This description of the spin-orbit angular momentum summation is known as $j - j$ coupling.

Under the $j - j$ coupling scheme the nomenclature is based on the principal quantum number n and on the electronic quantum number l and j mentioned above. In the historical X-ray notation, states with $n = 0, 1, 2, 3, 4, \ldots$ are designated K, L, M, N, ..., respectively, while states with various combinations of $l = 0, 1, 2, 3, \ldots$ and j =1/2, 3/2, 5/2, 7/2, ... are given conventional suffixes according to the listing in Table 2.1.

Table 2.1: X-ray and Spectroscopic Notation

Quantum numbers					
n	l	j	X-ray suffix	X-ray level	Spectroscopic level
1	0	$\frac{1}{2}$	1	K	$1s_{1/2}$
2	0	$\frac{1}{2}$	1	L_1	$2s_{1/2}$
2	1	$\frac{1}{2}$	2	L_2	$2p_{1/2}$
2	1	$\frac{3}{2}$	3	L_3	$2p_{3/2}$
3	0	$\frac{1}{2}$	1	M_1	$3s_{1/2}$
3	1	$\frac{1}{2}$	2	M_2	$3p_{1/2}$
3	1	$\frac{3}{2}$	3	M_3	$3p_{3/2}$
3	2	$\frac{3}{2}$	4	M_4	$3d_{3/2}$
3	2	$\frac{5}{2}$	5	M_5	$3d_{5/2}$
	etc.		etc.	etc.	etc.

The spectroscopic nomenclature is directly equivalent to the X-ray, and is more obviously related to various quantum numbers. In it the principal quantum number appear first, then states with $l = 0, 1, 2, 3, \ldots$ are designated s, p, d, f, ..., respectively, and follow the first number, and finally the j values are appended as suffixes. Thus the state written L_3 in the X-ray notation, in which n=2, l=1 and j=3/2, would be written $2p_{3/2}$ in the spectroscopic notation. In table 2.1 spectroscopic terms are listed opposite their X-ray equivalents.

The energy separation ΔE_j of the core level spin-orbit doublet peaks can be determined by experimental measurement or by theoretical calculation. In table 2.2, we give the splitting energies determined by photoemision spectroscopy for elements frequently used in semiconductors.

The relative intensities of the doublet peaks are given by the the ratio of their degeneracies $(2j + 1)$. Thus the area ratios and designations (nlj) or spin-orbit doublets are given in Table 2.3.

Table 2.2: Spin-Orbit Coupling Energy ΔE_j in eV[a]

	1s	2s	2p	3s	3p	3d	4s	4p	
^{5}B	--	VE *	VE						
^{6}C	--	VE	VE						
^{13}Aℓ	--	--	0.4	VE	VE				
^{14}Si	--	--	0.6	VE	VE				
^{15}P	--	--	1.0	VE	VE				
^{31}Ga	--	--	26.9	--	3.1	0.40[b]	VE	VE	
^{32}Ge	--	--	31.1	--	4.1	0.6	VE	VE	
^{33}As	--	--	35.5	--	5.0	0.69[b]	VE	VE	

[a] from Cardona and Ley (1978)

[b] from Bringans et al. (1987)

* valence electron

Table 2.3: Spin-Orbit Splitting Parameters

Subshell	j values	Area ratio
s	$\frac{1}{2}$	—
p	$\frac{1}{2}$, $\frac{3}{2}$	1 : 2
d	$\frac{3}{2}$, $\frac{5}{2}$	2 : 3
f	$\frac{5}{2}$, $\frac{7}{2}$	3 : 4

Chapter 3

Experimental

3.1 Si Surface Preparation And Characterization

As XPS is surface analytical technique, which probes samples to a depth of about 50 Å with Mg K_α radiation (1253.6 eV), the native surface oxides must be removed with proper care. Several different methods of surface preparation have been developed and used routinely in most laboratories. Among these, Ar^+ ion plasma cleaning is the most extensively used method. Ar^+ ion bombardment does efficiently remove the oxides, and the prepared samples can be transferred for XPS measurements without exposure to the atmosphere. However, the surface as well as subsurface layer structures can be damaged by the ions. For example, Lang and Taoufik (1986) have reported that Si surfaces are amorphized by Ar^+ ions at energies higher than 400 eV. This is substantialy lower than the normal Ar^+ ion-plasma source operation energy, which is generally >1 keV. The Ar^+ etched silicon surface is also found to be highly active due to the presence of Si dangling bonds, and to be easily attacked by O_2, H_2O, CO, etc., either in vacuum or atmosphere(Lu et al. 1988). Although the damaged layer can be recovered by subsequent annealing, this could potentially change the initial material structure.

Since the silicon structural properties are the subject of major interest of our studies, we found this method of sample preparation unsuitable for our studies.

More recently, scanning tunnelling microscopy (STM) studies showed (Swartzentruber et al 1989) that high quality c-Si surfaces can be prepared by heating the sample rapidly to 1250 °C and then following a slow cooling process. As we shall show in the next chapter, amorphous silicon begins to crystallize at annealing temperatures higher than 400 °C. In addition, the Ga-in-Si configurations and distributions vary significantly with the processing temperature. This method obviously doesn't fit our requirements. Other methods like cleaving, electric field desorption, etc., are also found very hard to be used for our studies.

After a series of studies, we found that wet chemical cleaning can produce a high quality Si surface. The cleaning procedures are: (1) the samples are ultrasonically cleaned with acetone and then methanol, then rinsed in de-ionized (DI) water; (2) etched in HF:H_2O (3:7) solution for 1 minute, diluted and rinsed in DI water, and then dried in flowing nitrogen. The chemistry of the etch reactions is (Fenner et al. 1989a,b)

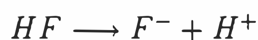

$HF \longrightarrow F^- + H^+$

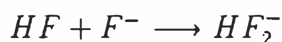

$HF + F^- \longrightarrow HF_2^-$

$3H^+ + 3HF_2^- + SiO_2(solid) \longrightarrow H_2SiF_6 + 2H_2O$

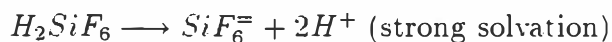

$H_2SiF_6 \longrightarrow SiF_6^= + 2H^+$ (strong solvation)

The prepared samples were transfered to the ultra-high vacuum (UHV) for low energy electron diffraction (LEED) and XPS measurements, and also for implantation of Ga, in less than 10 minutes. The quality of the prepared surfaces were characterized by LEED and XPS.

LEED is a technique in which electron beams with typical energy of about 100 eV are injected into a material. Some of the electrons are backscattered from the sample surface. Those backscattered electrons can form diffraction patterns. As we have discussed in the previous chapter, a moving electron interacts strongly

with other charged species in the material. This is usually described by the electron mean free path λ_e, which means the average distance that the electrons can cover without being inelastically scattered, and λ_e is found to vary with the electron kinetic energy as shown in Fig. 2.2. For a typical LEED electron with a kinetic energy of 100 eV, for example, the mean free path is about 10 Å . However, as LEED electrons must penetrate and then be back-diffracted from the material, the mean free path of the LEED electrons λ_e^{LEED} is therefore less that 5 Å . This means that only samples with well ordered first and second atomic layers can produce observable LEED patterns.

In Fig 3.1, we show a typical LEED pattern observed on Si(111) surfaces prepared by wet chemical cleaning. The first order diffraction pattern ('fuzzy' spots) has a 1×1 structure, but the beam width is larger than that of the second or higher order electron beams. We interpret this as due to a small deviations of the first atomic layer Si atoms from the ideal periodical arragement. The cause of such deviations is presumably from the residual contaminants like H, O, C, F etc.. From infrared spectroscopy studies, Chabal et al.(1989) have shown that HF treated silicon surfaces are covered mostly by hydrogen, along with small amount of oxygen and fluorine. Although we are unable to trace hydrogen distributions on our samples by XPS, we do find small amount of oxygen and carbon (less than 5 at.%) on the silicon surfaces through the measurements of O 1s and C 1s core level spectra, but no indication of silicon oxides is found from Si 2p core level spectra measurements. We believe the coverage of O and C is less than one atomic layer. The reason is that the periodicity of the first atomic layer will be totally destroyed by the forming of silicon oxides, of which the Si atom distribution is random or amorphous. Based on the same argument, we can conclude that any order of diffraction beams would not be observable if the oxides extended more than 3 atomic layer due to the limit of electron mean free path. We find LEED is a very good complementary technique to estimate the thickness of residual oxides

and contaminants, and we have used it to characterize chemically prepared GaAs surfaces(Lu et al. 1989a).

From the above discussion, we conclude that high quality silicon surfaces can be prepared by chemical etching. The residual contaminants, mostly silicon hydride, are only at the first atomic layer. The possible distortions of the bulk silicon structures by the processing acids are also limited to the first atomic layer. This has negligible effect on the XPS measurement, as the sampling depth is about 50 A, i.e. about 20 atomic layers deep from the surface.

The inert Si surfaces prepared by HF etching might relate to the existance of Si hydrides. Both high resolution electron energy loss spectroscopy (EELS) (Graf et al. 1989) and infrared spectroscopy (IR) (Burrows et al 1988 and Chabal et al. 1989) studies show that Si surfaces are almost completely covered by hydrogen, along with small amounts of oxygen and fluorine after being etched in buffered HF. The existence of Si-hydride on Si surfaces is found to restrict the oxidation rate(Lu et al. 1988 and Nakazawa et al. 1989). In Fig. 3.2 , we show Si 2p core level spectra of buffered HF etched a-Si:H and c-Si(111) samples exposed to atmoshere for various periods of time. The spectra show that the silicon oxide peak from c-Si samples is still very faint even after 7 days exposure to atmoshere. In comparison, the oxidation rate of a-Si:H is much faster than that of c-Si. This result is very surprising at first glance. as the Si dangling bonds in a-Si:H are passivated by H, and Si-H bonds are found responsible for a slow oxidation rate (Nakazawa et al. 1989) in c-Si. We attribute this to the existence of a buffered surface layer, with a thickness varing from 100 to 2000 Å depending upon the growth conditions(Fritzsche 1984), in a-Si:H films. This layer is 20 - 40% less dense than c-Si and is naturally quite porous(Fritzsche 1984), and is usually found contaminated with O and C as revealed by Auger electron spectroscopy and elastic-recoil studies(Sacher et al. 1984).

It was suggested by Fenner et al(1989a,b) that the passivation chemistry of

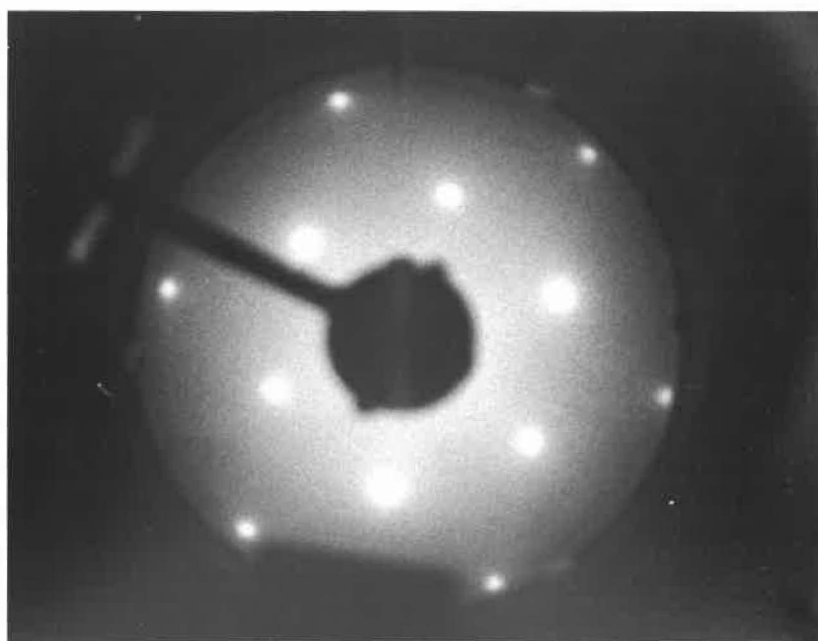

Figure 3.1: A typical LEED pattern oberved from a Si(111) surface prepared by the wet chemical cleaning method described in the text. The electron incident energy is about 80 eV.

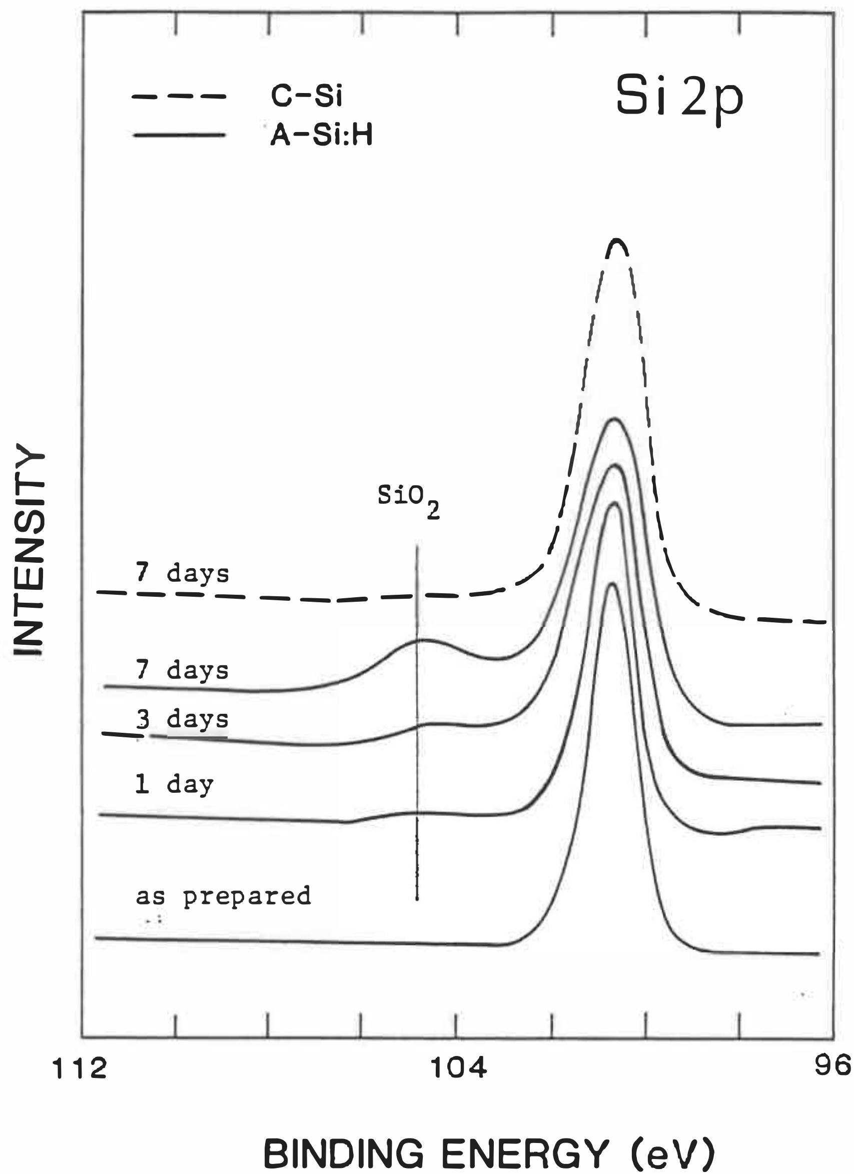

Figure 3.2: Si2p core level spectra recorded from a-Si:H and c-Si specimens. The sample surface was exposed to atmosphere for various lengths of time. The spectra were taken with Mg K_α radiation(1253.6 eV).

H–terminated silicon is likely due to the hydrophobic nature of such surfaces, the low Si–H bond ionicity, and its relative strength. These leave the H–terminated surface resistant to attack by F^- and OH^- ions at the liquid/solid interface and to chemisorption by H_2O, CO, etc. in vacuum or atmosphere. Physisorption and electrostatic binding of adventitious contamination and particulate matter is limited to the topmost atomic layer.

Although we cannot use LEED to characterize the wet chemically prepared a-Si:H samples, XPS measurements on both kinds of samples indicate the same amount of oxygen on the surfaces(Lu et al. 1988).

3.2 Implantation of Ga in Silicon

Samples of c-Si and a-Si:H substrates were used for the implantation. The a-Si:H was deposited on polished c-Si by silane (SiH_4) glow discharge (GD) at a substrate temperature of 250 °C. The details of the GD system and of the a-Si:H properties have been reported elsewhere(Brebner et al 1984). Samples of crystalline silicon were either (111) oriented and undoped, or (100) oriented and doped with P to a donor level of 10^{19} cm^{-3}. Before the implantation, the native surface oxides are efficiently removed using the wet chemical cleaning method described above.

The implantations were carried out with a VG MIG100 liquid metal ion gun (LMIG) mounted on the VG ESCALAB MK II system. The MIG100 is capable of implanting Ga, Au, Sn, Pb, Bi, In, and Cu over an energy regime of 1–10 keV.

Samples of c-Si and a-Si:H were implanted at normal incidence with 4 keV Ga^+ ions at 0.3 $\mu A/cm^2$ at room temperature, under a system vacuum of 8×10^{-10} torr. In situ XPS measurements show that about 15 at.% Ga(concentration distribution 50 Å from the sample surface) were implanted in 30 minutes. Samples of c-Si(111) and c-Si(100) were also implanted with 10 keV Ga^+ ions at 12.7 $\mu A/cm^2$ current

density, to study the Ga^+ distribution in silicon.

As the Ga^+ beam size increases with decreasing beam acceleration voltage or ion energy, we reduce the ion energy to the minimum of 4 KeV that can maintain stable operation of the LMIG. We have implanted Si with 4 KeV Ga ions with an area of 4×4 mm^2. The implanted region can be seen due to its milky appearance. The implanted region is much larger than the size of the X-ray beam(about 1 mm in diameter). In contrast, we found that the 10 KeV Ga^+ implanted region is less than 1×1 mm^2. In order to carry out XPS measurements, we usually have to implant 9 different spots to make a total area of 3×3 mm^2. This is very time consumimg. It takes about 5 hours to make one sample, and the LMIG also can not bear prolonged operation. The Ga planar distributions in silicon are unavoidably inhomogeous. So 10 KeV Ga^+ implanted samples are used only for profile studies.

XPS and Ar^+ ion sputter milling were used to profile implanted Ga. The Ar^+ sputtering was carried out in the instrument's preparation chamber at a pressure of 5×10^{-6} torr, ion energy of 6 keV, and beam current density of 30 $\mu A/cm^2$. The sputtering rate under these conditions was determined by measuring the sputtered depth d of a masked silicon sample versus sputtering time t, and is estimated at about (d/t=) 15 Å/min. The masking procedure for determining the sputtering yield consists of: (a) masking the Si sample surface with designed shape, which allows part of the sample surface to be attacked by Ar^+ ions. In current studies, we simply bond the surface with Cu tapes with a width of 1 mm in a parallel array with a span of 1 mm. (b) exposing the sample to Ar^+ ions for a period of time t, and (c) stripping off the Cu tapes and measuring the sputtered depth d in the unmasked regions. Then the sputtering rate can be estimated by d/t. Although we only estimated the sputtering rate in a c-Si sample, the sputtering rate in amorphous silicon should not differ much. Further, we do not need very high accurate data of sputtering rate in our studies. The entire process is illustrated

in Fig. 3.3.

After each etch, the samples were transferred to the analysis chamber for XPS measurements. The concentration of Ga was determined by measuring the intensity ratio of Ga3d to the total Ga3d and Si2p core levels, using sensitivity factors of 0.31 and 0.25 respectively (Briggs and Seah 1983), and by using the relation (2.9) given in the previous chapter. As the binding energy difference between Si 2p($\sim$ 100 eV) and Ga 3d($\sim$ 20 eV) is only $\sim$ 80 eV, the mean free paths of Ga 3d and Si 2p photoelectrons are essentially the same as shown in Fig.2.2. It also should be pointed out that the first data point in Fig.3.4 is taken with XPS, therefore it represent Ga concentration 50 Å from the sample surface before sputtering. The measured Ga distributions are shown in Fig 3.4. The profile clearly indicates that Ga atoms are distributed through the samples. The results suggest that the VG MIG100 LMIG mounted on the ESCALAB MK II system can be used for the low energy implantation of liquid metals such as Ga, despite the severity of sputtering effect at low implant energies.

Theoretical calculations of implanted Ga distributions in Si were also carried out using TRIM (transport of ions in matter), a Monte-Carlo simulation method developed by Ziegler et al.(1985). The results indicate a typical Gaussian distributions as shown in Fig. 3.5. This does not agree very well with the experimental profile shown in Fig.3.4. Based on SIMS measurements on numerous ions at low implantation energies from 2 to 20 KeV, Wach and Wittmaack(1983) also found non-Gaussian distributions of various elements in silicon.

3.3 Rapid Thermal Annealing

The samples were annealed using a commercial rapid thermal annealing apparatus (Heat Pulse 410) in a nitrogen atmosphere for 5 seconds at temperatures ranging from 250 to 350 °C for a-Si:H films, and 300 to 900 °C for c-Si samples.

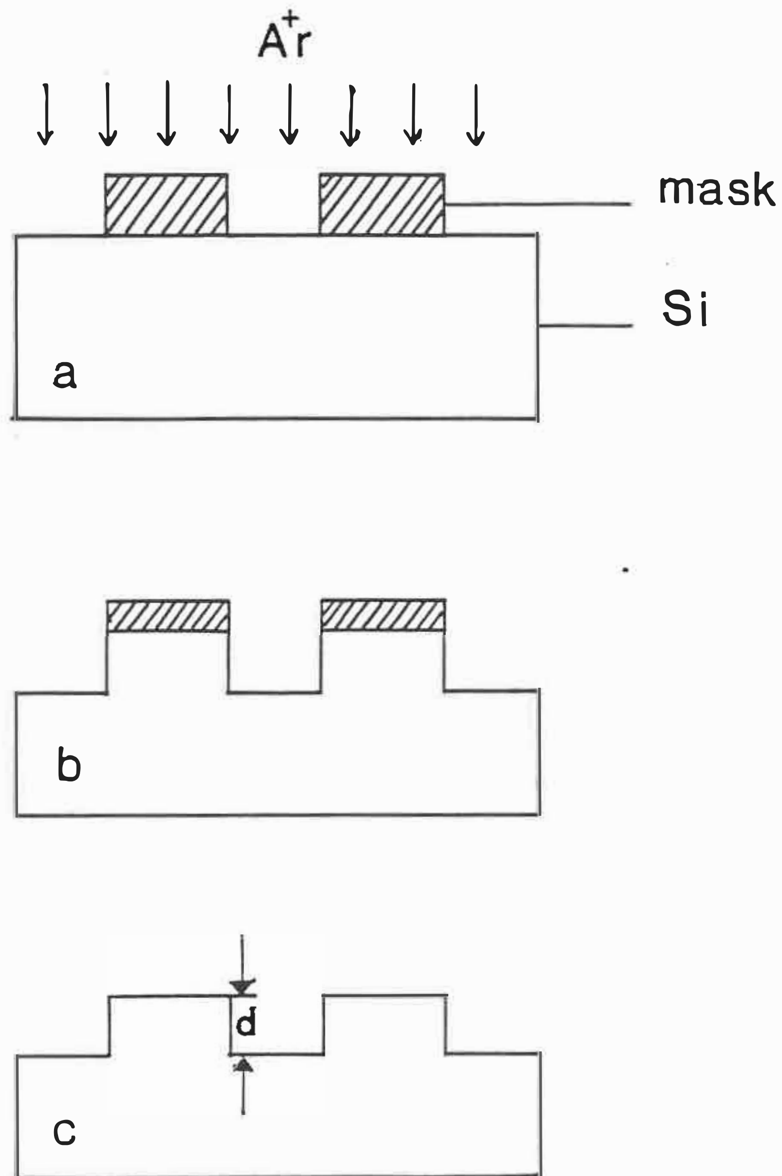

Figure 3.3: Illustration of the determination of the sputter-rate by the masking technique.

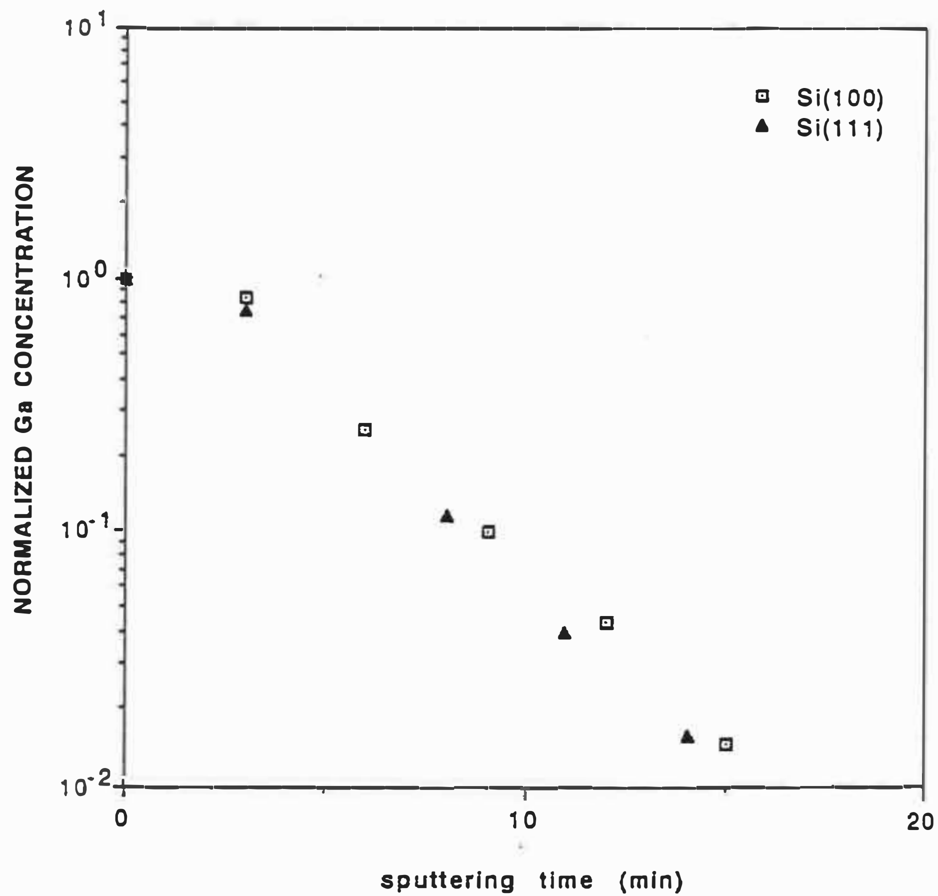

Figure 3.4: The distribution of ion-implanted Ga in Si measured by XPS and Ar^+ ion sputtering. The sputtering rate was about 15 Å/min.. The Ga^+ ions were implanted at normal incidence with beam current density of 12.7 $\mu A/cm^2$ and energy of 10 KeV.

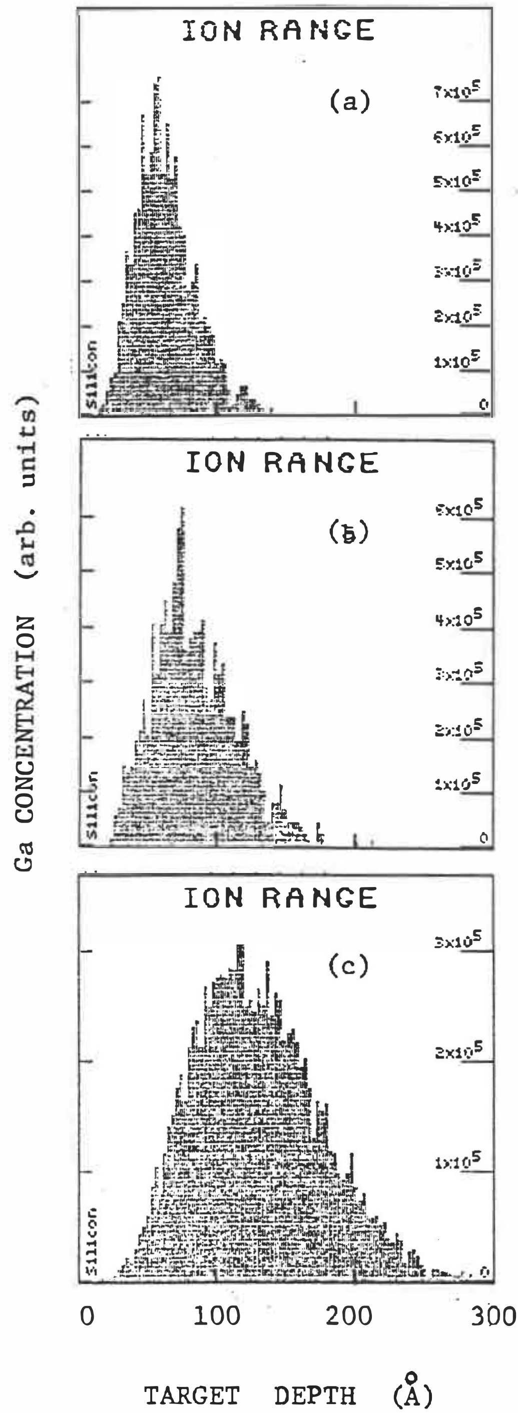

Figure 3.5: Calculated Ga profiles at ion incident energies of (a) 3 keV, (b) 5 keV and (c) 10 keV.

The a-Si:H films stripped off the substrate at annealing temperatures higher than 350 °C. This is possibly due to the crystallization of the film accompanied by strain release and changes in film density. Studies (Fiorini et al. 1987) on the RTA annealed a-Si:H, with an annealing time of 5s, show that most of the initial hydrogen stays in the film at the temperatures used.

3.4 X-Ray Photoelectron Spectroscopy

All valence band and core level spectra in this text were taken with the VG ESCALAB MK II (illustrated in Fig. 3.6) , using X-ray photoelectron spectroscopy (XPS). The system can provide two different photon beams with energies of 1253.6 (Mg K_α) and 1486.6 eV (Al K_α) using twin anode X-ray sources (TAXS). The photoelectron energies are measured by a concentric hemispherical analyser(CHA), as shown in Fig. 3.7.

As the Mg K_α radiation natural linewidth is 0.68 eV(Cardona and Ley 1978), which is narrower than that of Al K_α radiation, of 0.83 eV, it therefore provides better spectral resolution. On a well prepared crystalline silicon sample, for example, a full width at half maximum (FWHM) of 0.7 eV in the 2p core level can be obtained by using nonmonochromatic Mg $K\alpha$ radiation(see next chapter). The FWHM of Si2p photoelectrons is nearly equal to the natural linewidth of the Mg K_α radiation. To get such a 'good' resolution, however, it usually takes about one hour to accumulate a good signal-to-noise spectrum for an energy scan of 10 eV.

Experimental data were collected and processed by an IBM AT computer. The interface and software were developed by the GCM's ESCALAB, headed by Dr. E. Sacher. The valence band and Si2p and Ga3d core levels of the implanted and RTA annealed, as well as of virgin a-Si:H and c-Si samples were recorded and analyzed. The core level spectra were curve-resolved using a least-squares curve-fitting routine. The input parameters for deconvolution of various spectra

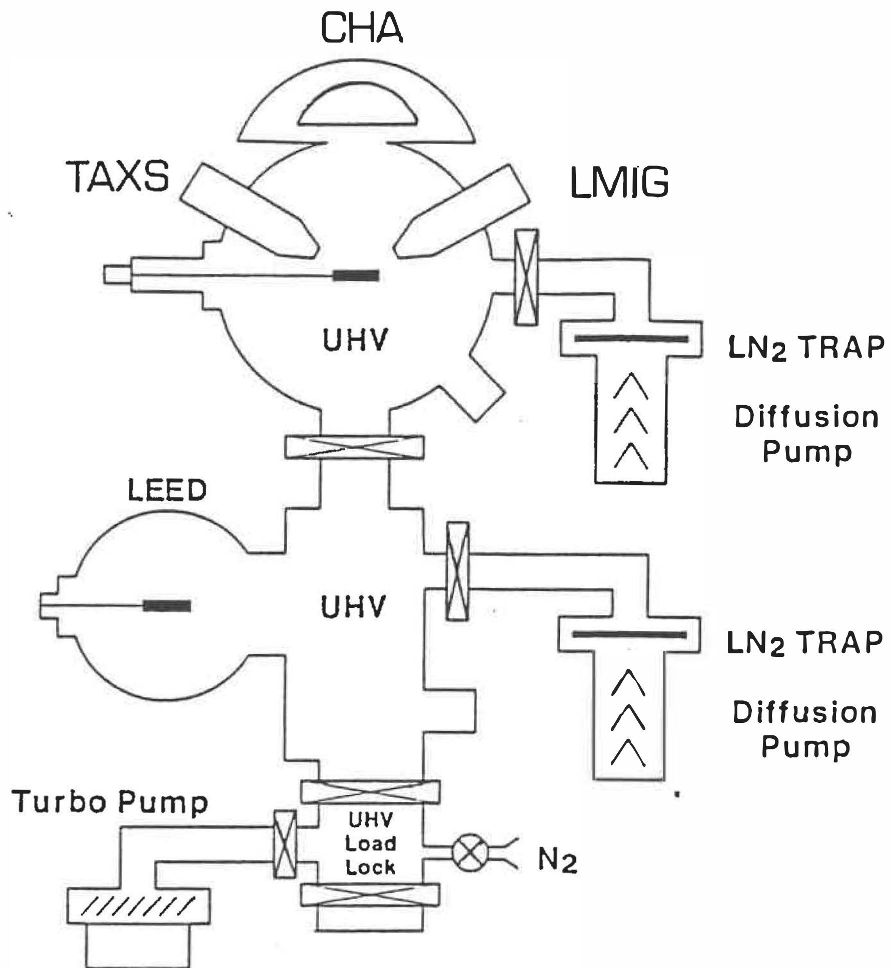

Figure 3.6: Illustration of the VG ESCALAB MK II instrument.

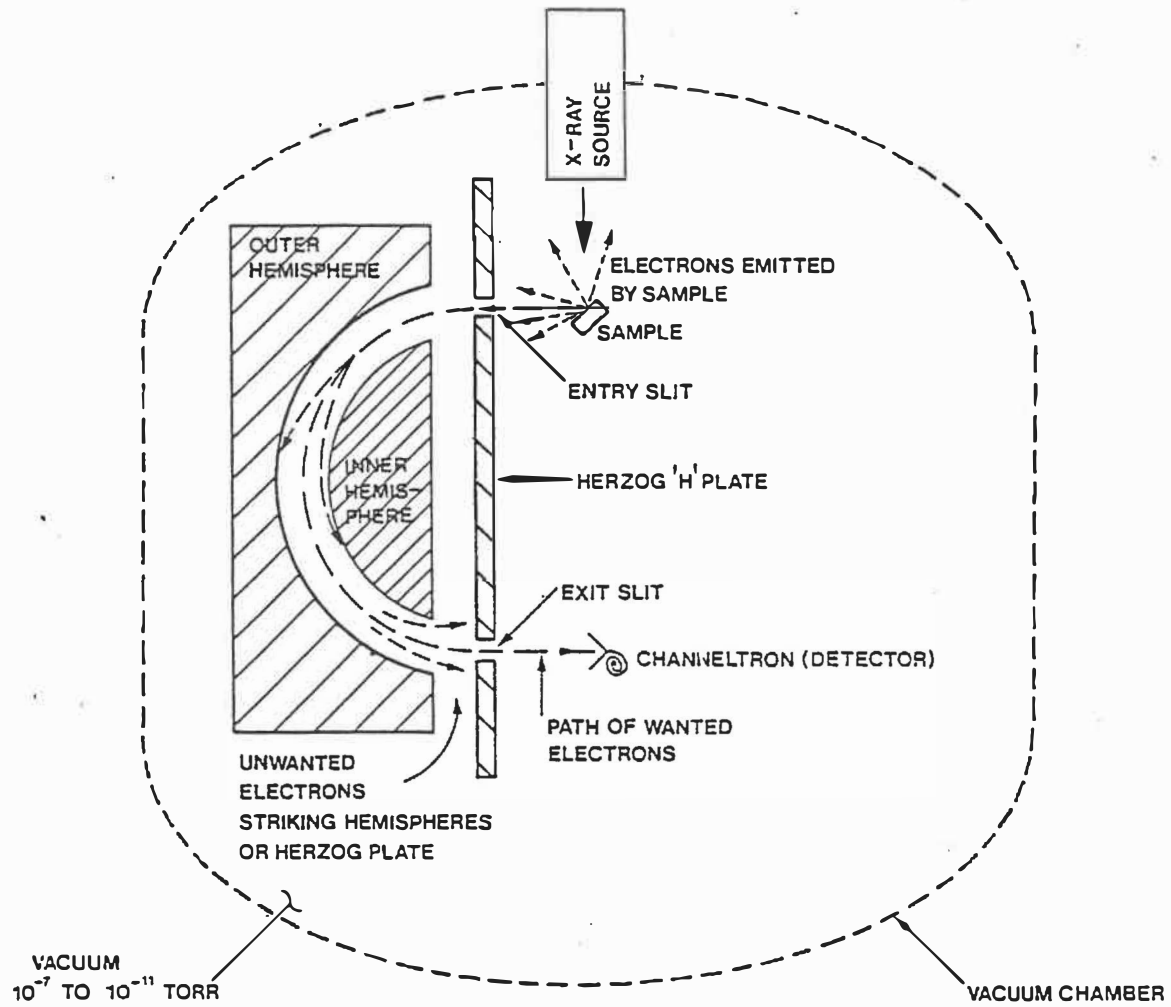

Figure 3.7: Illustration of the concentric hemispherical electron energy analyser.

will be presented in the relevent section of the following chapter.

Binding energies of metals are usually measured with reference to the instrument Fermi level. As resistance between the conducting metals and instrument is very low, the Fermi energies of metals and of the instrument are esentially the same, and can be easily determined on metals like palladium and nickel, which have sharp Fermi edges. The nickel valence photoelectron EDC(energy distribution curve) is shown in Fig. 3.8.

In semiconductors, electrons fill the valence band and the Fermi level lies in the band gap. The binding energy is commonly measured with reference to the valence band maximum (VBM), which is determined by extrapolation of the steepest descent of the leading edge. This is shown in Fig. 3.9. The binding energy reported in this text is measured relative to VBM, which is set at zero.

As the binding energies of Si 2p, Ga 3d and valence band electrons differ less than 100 eV, the mean free paths of the corresponding photoelectrons are essentially the same, as shown in Fig.2.2. This means that these electrons sampled all represent the structural properties of the same region. All of them have a sampling depth of 50 Å which primarily represents the bulk structural properties as discussed in the previous chapter.

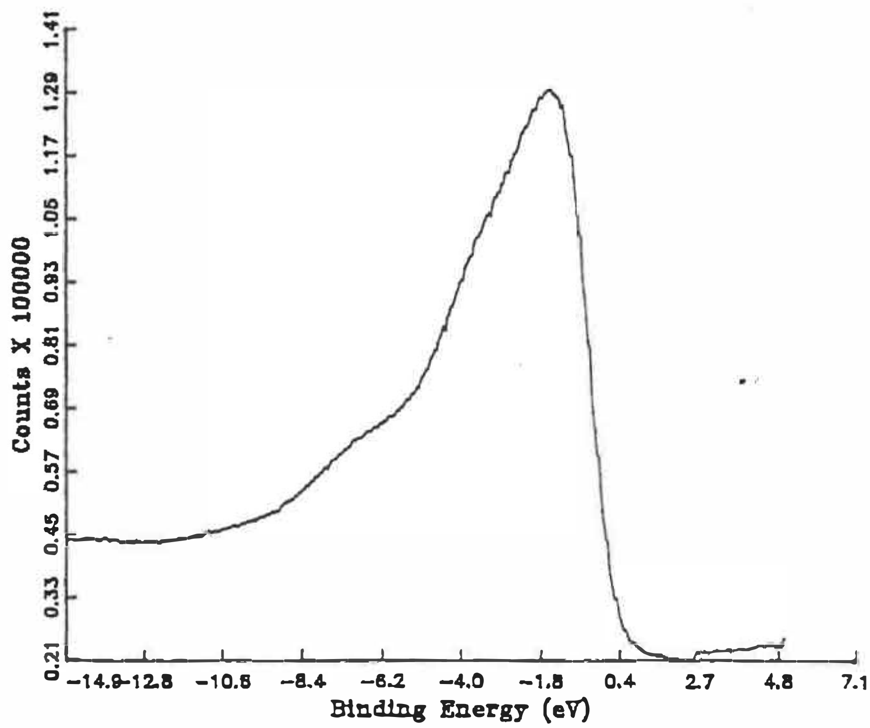

Figure 3.8: Nickel valence photoelectron EDC.

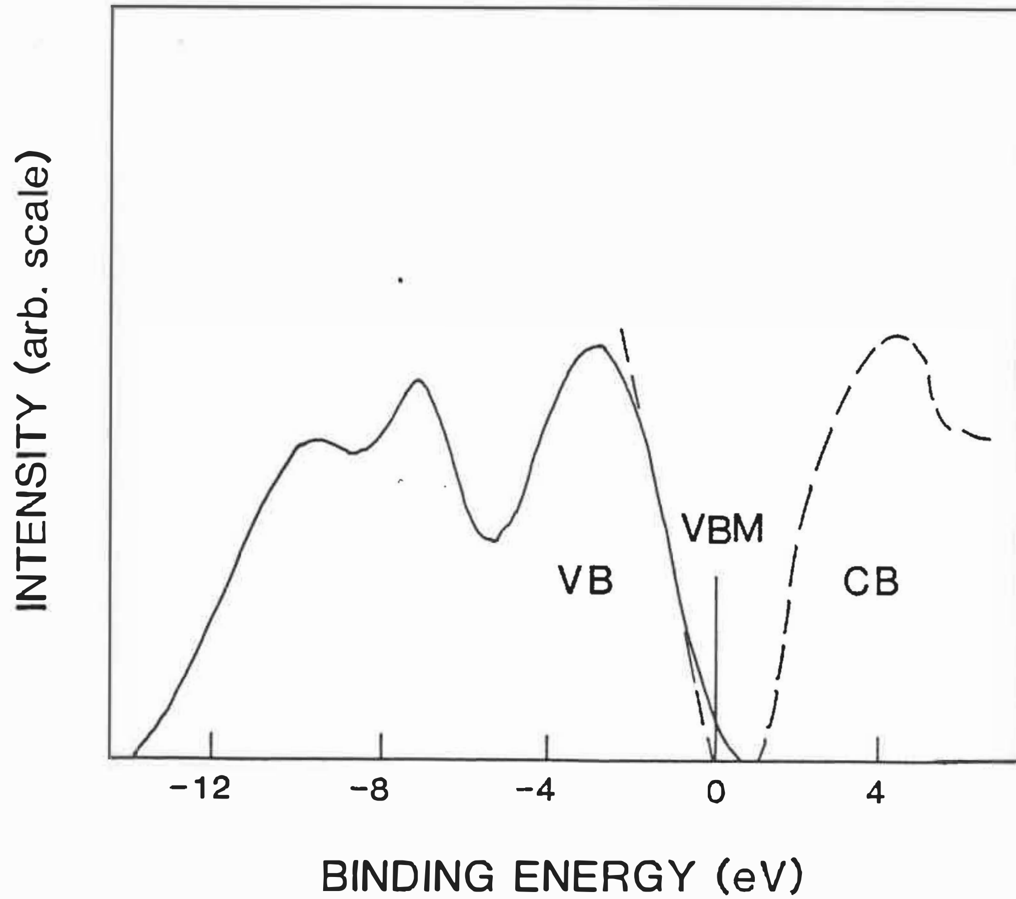

Figure 3.9: Photoemission valence band density of states (solid line) of c-Si. The empty conduction band is also illustrated in dashed curve. The VBM is shown to be determined by the extrapolation of the steepest descent of the VB leading edge, and is set at zero binding energy.

Chapter 4

Results and Discussion

4.1 Structural Relaxation and Crystallization of Amorphous Silicon Studied by Photoemission VB Spectroscopy

In Fig. 4.1, we show photoemission valence band (VB) density of states (DOS) spectra obtained from crystalline Si(100) and GD a-Si:H samples. The valence band maxima of the spectra are set at the zero binding energy position. The valence electron density of states N_v is shown in an arbitary scale. The inelastically scattered electron background of the spectra were removed using the method developed by Shirley(1976).

The four valence electrons of Si atoms are distributed among three peaks in the VB-DOS in such a way that the area under peak I corresponds to 2 electrons, and the areas under peaks II and III to one electron per Si atom each. States at the top of the valence bands are predominantly 3p-like and those at the bottom (peaks II and III) mainly of 3s character (Ley, 1984b, Bose et al. 1988).

Peaks II and III in the DOS of c-Si are related to the presence of sixfold rings in the diamond structure (Weaire and Thorpe,1971; Joannopoulos and Cohen, 1976).

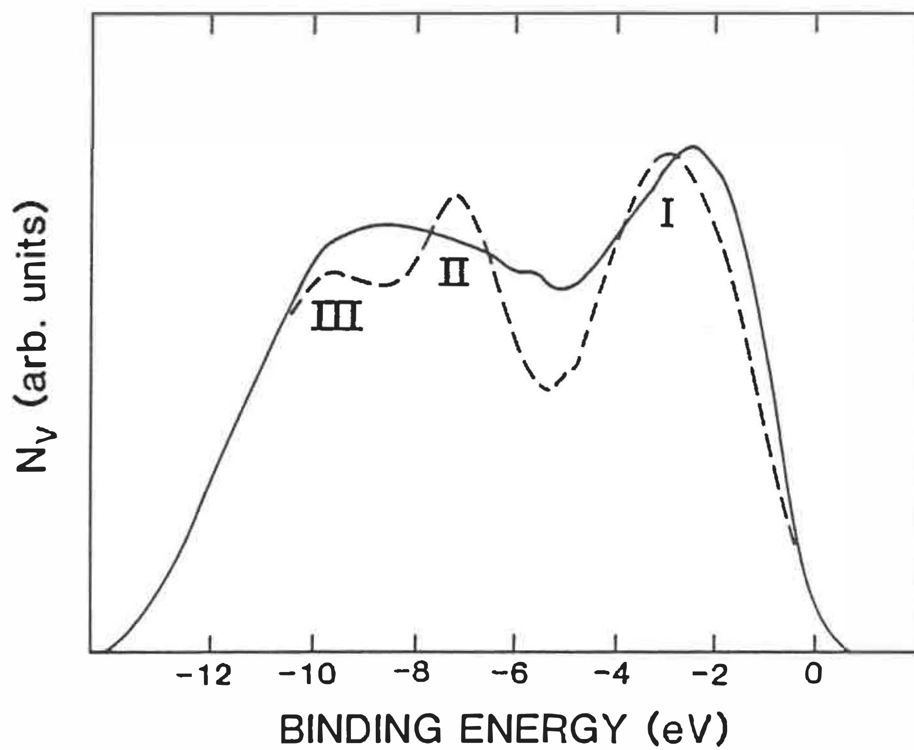

Figure 4.1: Experimental VB-DOSs of c-Si and a-Si:H derived from photoemission spectra. ——- a-Si:H; - - - - c-Si.

In models of the amorphous network, topological freedom of the atoms allows for five, seven, and perhaps eightfold rings while preserving the tetrahedral units. The most common five-fold rings, for example, can be formed with only a slight adjustment of the tetrahedral bond angle. It has been suggested by Weaire and Thorpe (1971) that five-fold rings should introduce states between those of peaks II and III and thereby fill the gap. This conjecture has been confirmed by a series of calculations(Joannopoulos and Cohen, 1976; Ortenburger et al, 1972; Ching et al, 1976, 1977). Therefore, the featureless appearance of the lower portion of the amorphous silicon DOS is due to an averaging of a variety of local bonding topologies.

The centroids of the 3p-like bands of states (peak I) of both c-Si and a-Si:H were determined by a curve-fitting method, with an accuracy of 0.1 eV. We find that the the centroid for a-Si:H has been shifted, compared to c-Si, by 0.4 eV towards the VBM. The same amount of shift has also been reported by Ley et al (1972). From their calculations, Joannopoulos and Cohen (1976) have concluded that the shift of peak I is due largely to bond-angle variations in the amorphous silicon continous random network (CRN).

In Fig. 4.3, we show the variations of VB-DOSs of Ga^+ ion-implanted a-Si:H with post-annealing at temperatures from 250 °C to 350 °C. We found that the 3s-like band density of states (peaks II and III) of samples annealed at 250 and 300 °C still form a simple hump, basically the same structure feature as observed on unimplanted a-Si:H except for a higher electron density of states at about 10 eV energy on the ion-implanted and annealed samples. The 'extra' density of states at about 10 eV energy is interpreted as being due to the contribution of implanted Ga. This will be discussed in the next section. Peaks II and III in the VB become distinct after an anneal at 350 °C. We attribute this to structural relaxation of the silicon CRN, which results in a more ordered silicon lattice and thereby reduces the density of states between Peaks II and III. This agrees with

the measurement of ΔE_{3p}, the centroid energy shift of the 3p-like band of states. The ΔE_{3p} measurement will be presented below.

Samples of a-Si:H thin film stripped off the c-Si substrates at annealing temperature ≥ 400 °C. This may be due to crystallization of the amorphous silicon network, which is accompanied by strain release and changes in the film density. Studies of reconstruction of the damaged silicon lattice and of the dopant activation process at higher post-annealing temperatures (≥ 400 °C) were, therefore, carried out only on c-Si samples. The valence electron energy distribution curves (EDCs) of Ga^+ ion-implanted c-Si are shown in Fig.4.3 as a function of annealing temperature. From the figure, we see that the general feature of the VB-DOS of a c-Si sample implanted and annealed at 300 °C is similar to that of amorphous silicon, as discussed above. However, typical crystalline silicon VB-DOS features are found for all valence electron spectra obtained on samples annealed at temperatures ≥ 400°C. The centroid of the 3p-like band of states of these samples is also found at the same energy as that of unimplanted c-Si(see details below). LEED was used to examine the crystallinity of the sample surfaces. Diffraction spots can only be observed on samples annealed at temperatures ≥ 500 °C. We thus conclude that the damaged silicon crystallizes at annealing temperature $\geq$ 500 °C. The two distinct 3s-like peaks observed for samples annealed at 400 °C indicate that the silicon CRN is subject to a structural relaxation process prior to crystallization.

As discussed above, the energy location of the centroid of the 3p-like band is one of the characteristic parameters distinguishing the valence electron distributions of the Si crystalline lattice and the amorphous CRN. Values of ΔE_{3p}, the centroid energy shift of the ion-implanted and annealed c-Si and a-Si:H samples (compared to unimplanted c-Si) are given in Table 4.1. From the table, we can see that the binding energies of virgin a-Si:H, as implanted a-Si:H and c-Si, and implanted a-Si:H and c-Si samples annealed at temperatures ≤ 300 °C are all the

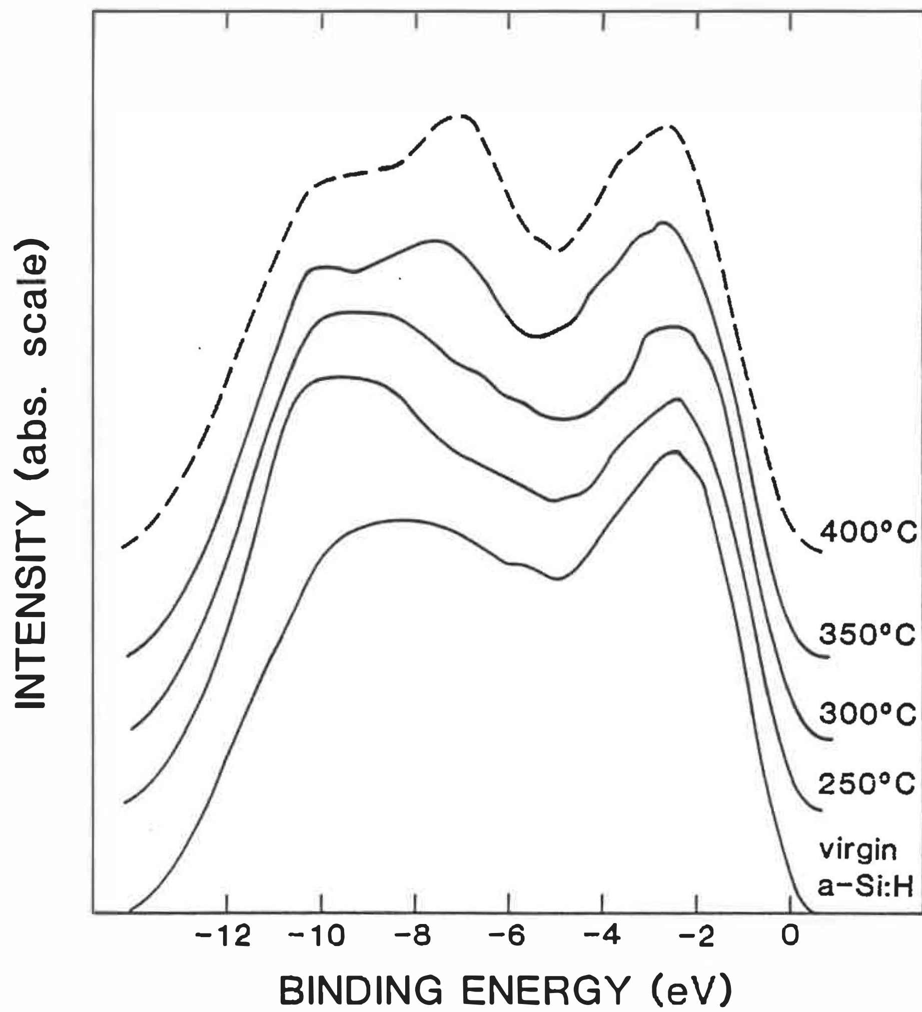

Figure 4.2: VB-DOS of Ga ion-implanted and annealed a-Si:H. The dashed curve is obtained on a c-Si sample.

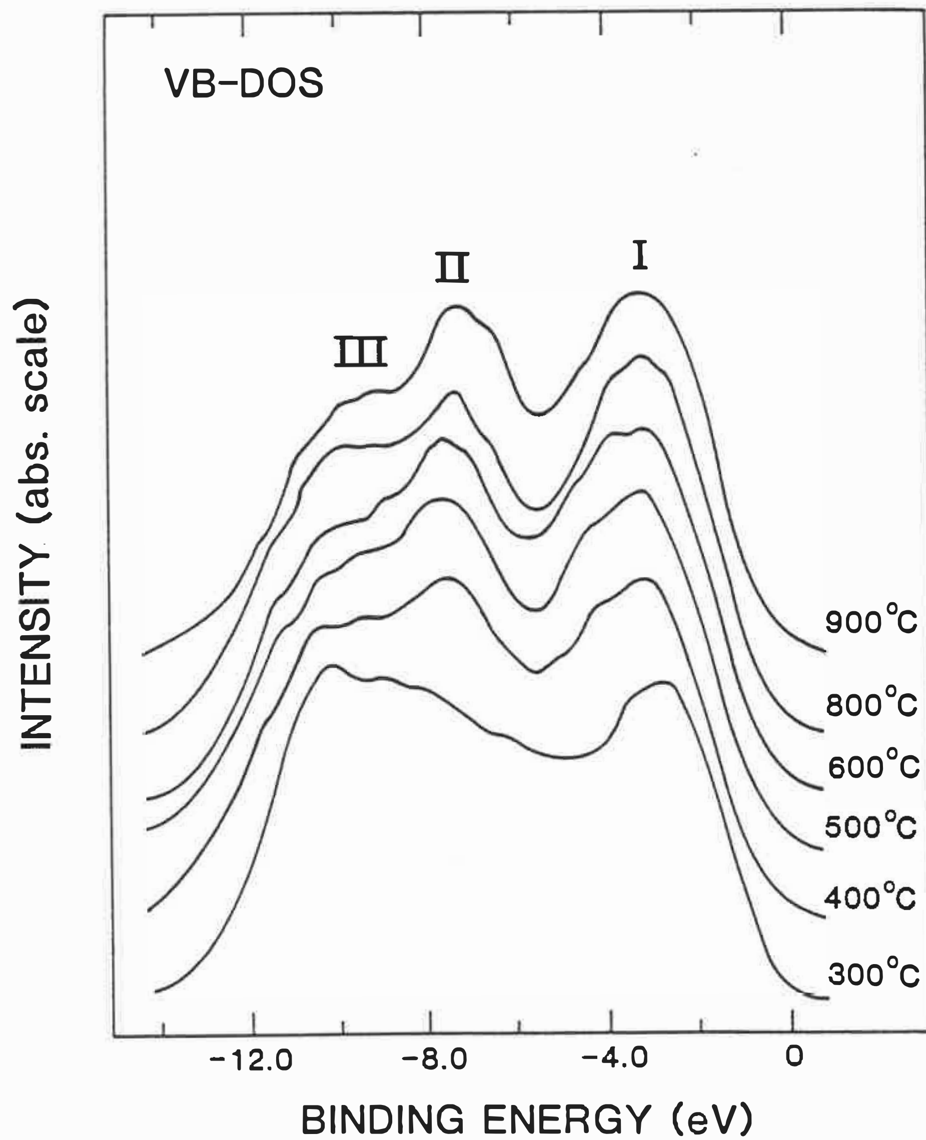

Figure 4.3: VB-DOS of Ga ion-implanted and annealed c-Si. The valence band maxima are aligned at 0 eV.

same. The centroid of the 3p-like peak of all these samples is shifted towards the top of the valence bands by 0.4 ± 0.1 eV, compared to virgin c-Si. For samples annealed at 350 °C, ΔE_{3p} is reduced to 0.1 eV. After an anneal at temperatures ≥ 400 °C, it is reduced to zero. This again suggests that the damaged silicon crystallizes at annealing temperatures ≥ 500 °C, and that the silicon CRN undergoes a structural relaxation or bond-angle ordering prior to crystallization.

From Raman scattering and neutron-diffraction studies, Fortner and Lannin (1988, 1989) also concluded that Ar^+ ion amorphised Si and Ge lattices transformed to a more ordered structure by way of structural relaxation upon annealing. $\Delta\theta$, the average Si-Si bond-angle variation or the width of Si CRN bond-angle distribution function P(θ), was found to decrease about 2° (Fortner and Lannin 1988 and 1989) for ion-amorphized Si and Ge upon annealing at 350 °C. The bond-angle deviation stored elastic potential energy release, which is brought about by structural relaxation or bond-angle ordering, was also measured on ion-implanted Ge (Donovan et al. 1985) and more recently on ion-implanted Si (Roorda et al 1989, Jacobson et al 1989) by differential scanning calorimetry (DSC) experiments. Structural relaxation and lattice ordering prior to crystallization, were also studied on low temperature deposited and post-annealed a-Si and a-Ge CRN using Raman scattering and extended X-ray-absorption fine-structure (EXAFS) experiments (Paesler et al 1983 and Tsu et al 1984).

4.2 VB-DOS Variations with Ga Atomic Orbital Hybridization

One interesting feature of VB-DOS of ion-implanted Si is that there is a significant increase in the density of states at the bottom of the VB at an energy ~ 10 eV, as shown in the EDCs of Fig. 4.2 and 4.3. This can be more easily seen in Figure 4.4, where we have aligned the 3p-like band density of states N_v to

Table 4.1: ΔE_{3p} as a function of annealing temperatures.

TEMPERATURE (°C)	500	400	350	300	250	as-implanted	virgin
ΔE_{3p} (eV) (a-Si:H)			0.1	0.4	0.4	0.4	0.4
ΔE_{3p} (eV) (c-Si)	0.0	0.0		0.4		0.4	0(reference)

the same value. This clarifies changes in density of states in the 3s-like, peak-III, region.

We believe that the 'extra' density-of-states in this region is due principally to the two 4s electrons of unactivated, free, or elementary gallium Ga^o. The binding energy of the $Ga^o 4s^2$ electrons is 11.55 eV (see Table 4.2) , roughly the same energy at which we found an increased density of states. The 4p electrons of Ga^o, have a binding energy of 5.67 eV. The $Ga^o 4p^1$ electron, however, did not produce any significant features in the EDC's shown in Fig. 4.4. This may be due to the 4p electron of Ga atom having a lower photo-electric cross section than the 4s electron, as shown in Fig. 2.3. In addition, the Ga 4p orbitals are only half filled.

We shall show in the following section that the valence electrons $4s^2 4p^1$ of Ga atoms are promoted to either an sp^2 or an sp^3 hybrid with increasing annealing temperature. This corresponds to a decrease in free gallium valence electrons, and consequently a decrease in the density of states in the region of peak III, as shown in the figure. The Ga atoms also diffuse upon annealing (the change in Ga concentration will be discused in later sections).

We are unable to identify any additional density of states contributed by newly created sp^2 and sp^3 Si-Ga bonding states in the EDCs of Fig. 4.4. This may be because the number of hybridized Ga is small at annealing temperature at or below 400 °C(see Section 4.4). For samples annealed at 500 °C, however, 10 at.% tetrahedral sp^3 Ga has been found in the Si matrix through measurements of the Si2p core level(see section 4.6). The supersaturated tetrahedral Si-Ga bonding state , however, does not produce a distinct feature in the EDCs. Although there is no quantum chemical or energy band calculations of our specific case available at the time of writing, we believe that the energy distributions of the electrons at Si-Si and Si-Ga bonds should be similar because both of them are described by a non-localized Bloch wave function in a periodical Si lattice arrangement. An increase in the absolute value of the VB density of states, however, would

VB-DOS

Nv (arb. units)

Gå4s²

Gå4p¹

−12 −10 −8 −6 −4 −2 0

BINDING ENERGY (eV)

Figure 4.4: VB-DOSs of virgin a-Si:H, ——; Ga ion-implanted and annealed at 250 °C, - - - -, and 350 °C, - · - · - · -; Ga ion-implanted c-Si annealed at 500 °C, ······.

Table 4.2: Hartree-Fock s- and p-orbital energies in eV(Harrison 1981).

	Si	B	Al	Ga	In	Tℓ
-E(s)	14.79	13.46	10.70	11.55	10.14	9.82
-E(p)	7.58	8.43	5.71	5.67	5.37	5.23
$-E(s^2p^1)^a$	12.39	11.78	9.04	9.59	8.55	8.29
$-E(sp^2)^b$	9.98	10.11	7.37	7.63	6.96	6.76
$-E(sp^3)^c$	9.38	9.69	6.96	7.14	6.56	6.34

a Calculated as $E(s^2p^1) = 2/3Es + 1/3Ep$

b Calculated as $E(sp^2) = 1/3Es + 2/3Ep$

c Calculated as $E(sp^3) = 1/4Es + 3/4Ep$

be expected simply due to the fact that real space silicon density is increased by the introduction of Ga atoms. To measure the absolute N_v, nevertheless, is a non-trivial experiment.

The tetrahedral Si-Ga bonds do affect the VB-DOS by moving it toward the vacuum level. This will be disscussed in detail in Section 4.6.

4.3 Ga Coordination Numbers in Amorphous Silicon Determined by Core Level Photoemission Spectra

We discussed in Chapter 2 that valence electron redistributions brought about by the forming of different chemical bonds will lead to changes in the core level binding energy, or a chemical shift. As gallium has an electronegativity of 1.13 (Phillips scale; Phillips 1973), which is lower than that of Si, at 1.41, we would expect the Ga3d core levels to shift to higher binding energy with the formation of Si-Ga bonds.

In Fig. 4.5, we show Ga3d core level spectra recorded on as-implanted and annealed c-Si samples The spectra become very faint on samples annealed at temperatures ≥ 500 °C, and the signal-to-noise ratio is too weak for any quantitative analysis. The Ga3d core levels were curve-resolved using a least-squares curve-fitting method. The input data for the Ga3d core level doublet are the spin-orbit splitting energy of 0.4 eV, an intensity ratio of $3d_{3/2}$ to $3d_{5/2}$ of 2:3, a full width at half maximum (FWHM) of the convolving function of 1.2 eV, and a Gaussian to Lorentzian mixing ratio of 0.6. The above parameters were found to best fit the experiment data, and were fixed for all Ga3d core levels.

In Fig. 4.5, the deconvoluted peaks are shown as dashed curves, which are the sums of the $3d_{3/2}$ and $3d_{5/2}$ spin-orbit doublets. The sums of these deconvoluted

peaks are shown as dotted curves. The experimental data are shown as solid lines.

For as-implanted samples. two peaks, at binding energy of 18.8 and 19.5 eV, were found to best fit the experimental data, as shown in the figure. For annealed samples, however. three peaks at binding energies of 18.8, 20.0 and 21.1 eV (with an accuracy of 0.1 eV) were deconvoluted. The positions of each of these peaks were obtained from different samples and confirmed by measuring the energy difference between $Si2p_{3/2}$ and $Ga3d_{5/2}$ lines.

The peak at 18.8 eV corresponds to elementary gallium Ga^{o}(Bringans et al 1987). We assign the chemically shifted peaks at energies of 19.5 and 20.0 eV, to Ga^2 and Ga^3, which are two- and three-fold coordinated gallium bonded to Si, respectively. The chemical shifts of Ga^2 and Ga^3 of 0.7 and 1.2 eV are in good agreement with synchrotron radiation measurements (Bringans et al 1987) on Si surfaces covered with Ga. We interpret the peak at 21.1 eV with a chemical shift of 2.3 eV, as the 4-fold coordinated substitutional gallium Ga^4. We have pointed out in Chapter 3 that the sample surface contaminants are less than one atomic layer while the sampling depth of XPS is about 25 atomic layers . This makes it unlikely that the peak with a 2.3 eV chemical shift is due to Ga oxides. Further, the Ga oxides, if any, should have a chemical shift of 1.3 eV. as we reported elsewhere (Lu et al 1988, 1989).

The chemical shift per Si-Ga bond can be calculated by dividing the decovoluted chemical shift by the coordination numbers of the corresponding peak. This gives the chemical shift per Si-Ga bond of 0.35. 0.4. and 0.59 eV for Ga^2 ,Ga^3, and Ga^4, respectively. The significantly large shift per Si-Ga bond for Ga^4 state may be explained by its specific orbital properties. As a subsititutional dopant in the Si matrix, the Ga atom has to draw an extra electron from somewhere in the material to form the tetrahedral sp^3 hybrid orbital state Ga^4. The Ga^3, however, is believed to be a trigonal sp^2 hybrid in the amorphous silicon CRN

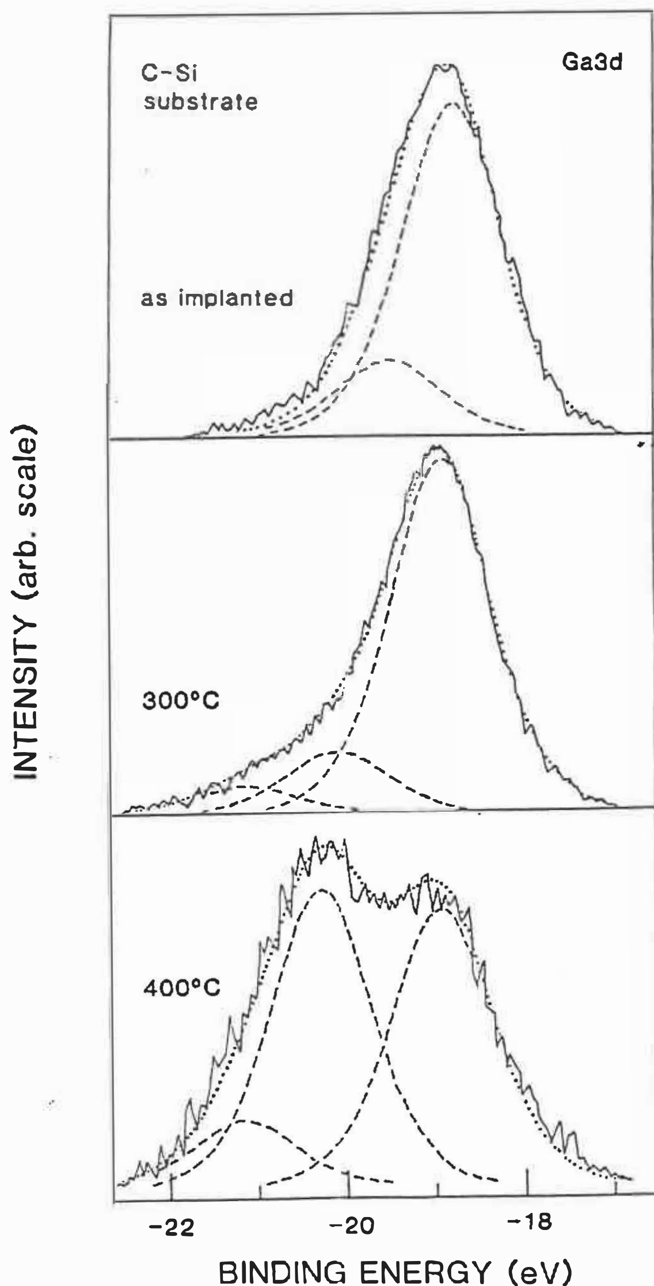

Figure 4.5: Ga3d core level spectra measured on c-Si samples, as-implanted, and annealed at 300 and 400 °C. The experimental signals are shown by solid line. The dashed curves show the results of deconvolution into different components and the dots are the sums of the components. Intensities are shown on an arbitary scale.

(Robertson 1983). It is well known that the electronegativity depends strongly upon the orbital hybrid state; since s electrons are bound more tightly than are p electrons, the electronegativity of an atom increases with the s character of the orbit (Huheey 1978). In Fig. 4.6. we show the electronegativities of carbon, nitrogen and oxygen as a function of s character. Electrons in an sp^3 hybrid with 25% s character, have a lower electronegativity than electrons in an sp^2 state with 33% s character. This means that Ga^4 will lose more electrons to Si atoms, which remain sp^3 hybridized, than does Ga^3, and consequently a larger chemical shift is expected from the tetrahedral Ga-Si bond. The smallest chemical shift of Ga^2 leads us naturally to think that it may be the linear sp hybrid.

The annealing activated, 3- and 4-fold coordinated, Ga are also observed on ion-implanted a-Si:H samples. In Figure 4.7, we show the Ga3d core level electron spectra recorded on ion-implanted and annealed a-Si:H. The three deconvoluted peaks correspond to (from right to left) Ga^o, Ga^3 and Ga^4 respectively. The binding energies and chemical shifts of these peaks are the same as those observed on c-Si samples.

It is interesting to note that most of the as-implanted Ga atoms are in the elementary state, along with very small amounts of Ga atoms 2-fold bonded to the damaged Si lattice. The 2-fold coodinated Ga configuration is an unstable state and disappears on annealing. Because of the amorphous nature of the ion-implanted and low temperature annealed (≤ 400 °C) silicon lattice, the anneal-activated Ga atoms can occupy either 3- or 4-fold coordinated sites. This is due to large Si-Si bond-angle and bond-length deviations in the amorphous silicon CRN. For a well reconstructed crystalline silicon lattice after an anneal ≥ 500 °C, however, only tetrahedral Ga (aside from interstitial gallium) is allowed, due to topological constraints(see section 4.6).

It should be pointed out that Ga 3d signals from samples annealed at temperatures higher than 500 ^{0}C become too weak to be detected using normal data

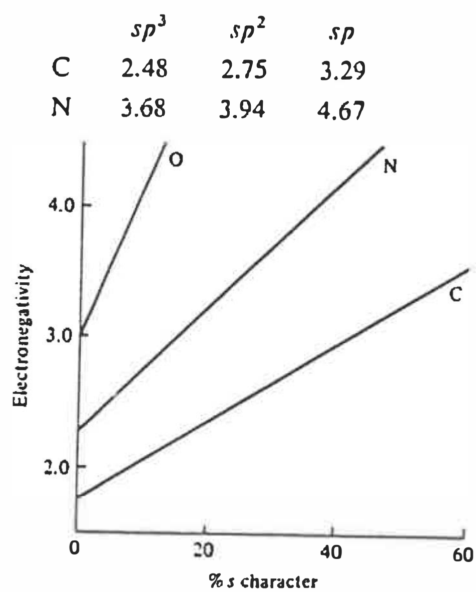

Figure 4.6: Electronegativities of carbon, nitrogen and oxygen as a function of percent s character(Hueey (1978)).

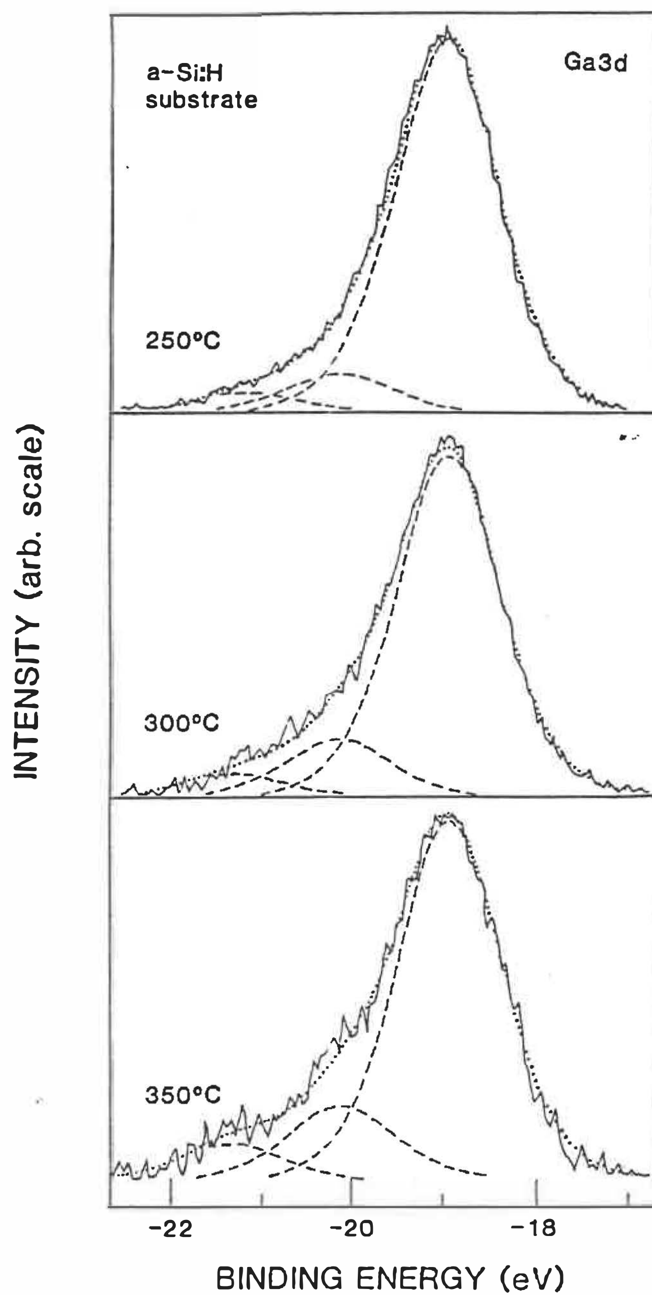

Figure 4.7: Ga3d core level spectra measured on ion-implanted and annealed a-Si:H samples. The experimental signals are shown by solid lines. The dashed curves show the results of deconvolution into different components and the dots are the sums of the components. Intensities are shown on an arbitary scale.

accumulation times (about one hour for an energy scan of 10 eV). We have not attempted to record Ga 3d spectra of those samples. In a similar study of As^+-implanted Si (with an As dose of $\sim$ 3 at.%), Lau (1989) has found that it takes about 5 hours to record an As 3d core level spectrum with reasonable signal-to-noise ratio.

4.4 Activation of Ion-Implanted Ga Atoms and Doping Efficiency of Amorphous Silicon

In Table 4.3. we show fractions of differently coordinated Ga in Si as well as the total Ga concentration shown in Figs. 4.5 and 4.7. In Fig. 4.8, we show the logarithm of Ga^3/Ga and Ga^4/Ga as a function of reciprocal annealing temperature. Ga^3/Ga and Ga^4/Ga, which means the fraction of 3-fold or 4-fold coordinated gallium, are obtained simply by dividing the intensity of the Ga^3 or Ga^4 peak by the sum of the intensities of all the deconvoluted peaks. From Table 4.3 and Fig. 4.8 we can see that both Ga^3 and Ga^4 concentrations increase with annealing temperatures, and that the number of activated Ga^3 atoms is approximately twice that of Ga^4 atoms, in both a-Si:H and c-Si samples, for the temperature range of 250 to 350 °C. The variations of Ga^3/Ga and Ga^4/Ga with annealing temperature T_a can be fitted to the form

$$Ga^{3,4}/Ga \propto e^{-E_a/kT_a} \tag{4.1}$$

where $Ga^{3,4}$ means either Ga^3 or Ga^4, and E_a is an activation energy. This yields an activation energy of 0.14±0.05 eV for both three- and four-fold coordinated Ga atoms over the temperature range of 250 to 350 °C.

Fortner and Lannin (1988) have reported an activation energy of 0.16 eV for the heat, H_{SR}, released upon structural relaxation during an anneal of ion-implanted Si and Ge, from room temperature to 325 °C. On the basis of Raman scattering

Table 4.3: Fractions of Differently Coordinated Gallium, (Ga^i/Ga), and Total Ga Concentrations, C, Measured after Annealing at Various Temperatures[a].

Ta (°C)	250	300	350	400
Ga^0/Ga	0.85	0.82 (0.78)	0.77	(0.43)
Ga^3/Ga	0.10	0.13 (0.14)	0.15	(0.47)
Ga^4/Ga	0.05	0.05 (0.08)	0.08	(0.10)
C (at.%)[b]	15 (15)	12 (11)	6	(9)

a) Values in parenthese are for c-Si; other values are for a-Si:H

b) The Ga concentration was determined by $Ga3d_{5/2}$ and $Si2p_{3/2}$ core level peak intensities with sensitivity factors of 0.31 and 0.25 respectively (Briggs and Seah 1983).

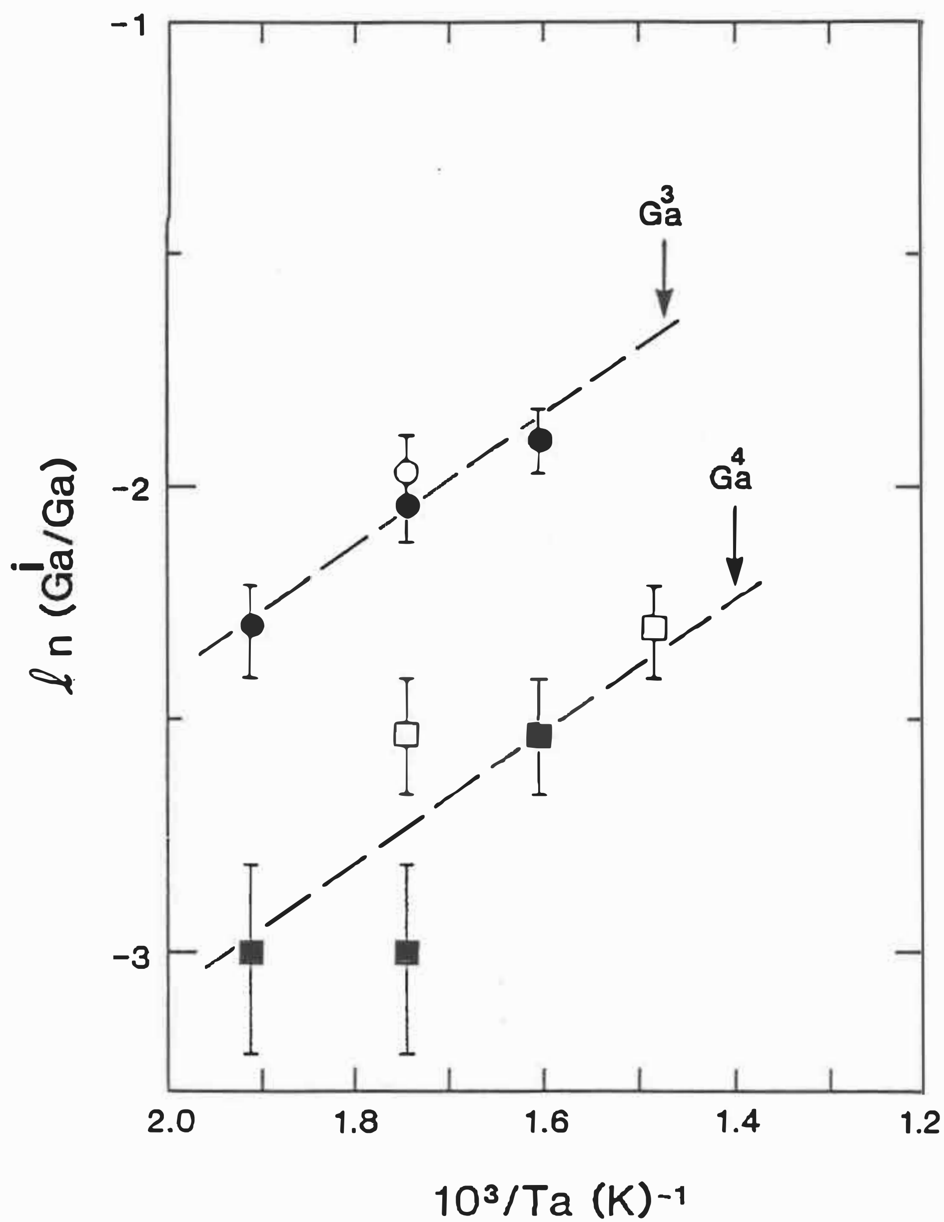

Figure 4.8: Variations of three- and four-fold coordinated Ga^i components (Ga^3/Ga and Ga^4/Ga) as a function of annealing temperature T_a. Data are measured on c-Si (solid circles and squares) and a-Si:H (open circles and squares).

experiments, they concluded that H_{SR} is the stored elastic potential energy released upon the relaxation of the bond angle deviation through the relation $H_{ij} = C(\Delta\theta_i^2 - \Delta\theta_j^2)$, where C is a constant, $\Delta\theta$ is the deviation, and i and j refer to the initial and final state in the annealing process.

The activation energy we found is quite close to that reported by Fortner and Lannin. This suggests that H_{SR} is the primary energy source promoting the Ga into sp^2 or sp^3 bonding states. This relaxation also affects the valence electron density of states spectra, as discussed above.

In Table 4.2, we show the energies of different orbital states. From the table we see that the energy difference between sp^2 and sp^3 is 0.49 eV, while the energy differences between the s^2p^1 state and sp^2 and sp^3, are 1.96 and 2.45 eV, respectively. It is possible that the barriers to s^2p^1-to-sp^2 and to (s^2p^1 + e^-)-to-sp^3 conversion might differ only slightly so that the activation energy of 0.14 eV is observed in both cases. The energy of the sp^2 orbit is lower than that of the sp^3 orbit. This may explain why the number of activated 3-fold coordinated Ga atoms is higher than that of substitutional gallium atoms.

One of the most important and most controversial physical parameters in amorphous semiconductors is the solid-phase doping efficiency, η_{sol}. This is defined as the number of donors or acceptors, which are presumably 4-fold coordinated dopants N_4(Robertson 1983, Stutzmann 1986), divided by the total dopant concentration N_o(Stutzmann 1986). That is, Ga^4/Ga in our studies. The core level spectral measurements in Table 4.3 indicate that η_{sol} varies from 5% to 10% for Ga concentrations ranging from 15 at.% to 6 at.%.

Various experimental techniques have been used deduce the doping efficiencies. EXAFS and NMR measurements on As and P in a-Si:H suggested that 4-fold coordinated donors could be as numerous as as 20% for samples with total concentrations around 1 at.% (Knights, Hayes and Mikkelsen 1977; Reimer and Duncan 1983). This is believed to be overestimated (Stutzmann 1986, Street et al

1988). Based on electrical measurements, however, Stutzmann (1986) and Jousse et al (1987) showed that the solid-phase doping efficiency is less than 10% for various dopants over a wide range of doping levels. We found that the doping efficiency estimated by Stutzmann and Jousse et al is consistent with our experiment results. That is, the doping efficiency is generally less than 10%.

4.5 Amorphous Silicon Doping Mechnism

In 1967, Mott introduced "8-N" (N is the number of valence electrons) rule to account for the absence of doping in covalent, amorphous chalcogenide semiconductors. The suggestion was that element coordinations in an amorphous network satisfy their valence requirements locally in the absence of constraints due to periodicity: electrons are paired and the bond number n_c obeys the "8-N" rule, that is, n_c=8-N for N>4 and n_c=N for N<4. Thus the coordination of Si is 4, of Ga is 3, etc.. When, in 1975, Spear and LeComber showed that hydrogenated amorphous silicon (a-Si:H) could be substitutionally doped by the addition of small amounts of phosphine and diborane to the silane plasma, however, this discovery came as a surprise to many workers in the field. The "8-N" rule has since been regarded to be inadequate to explain the doping of amorphous Si and Ge. In 1982, Street proposed a modified "8-N" auto-compensation doping model. He proposed that the occurrence of 4-fold coordinated dopants is associated with the production of defects, in order to prevent a violation of the "8-N" rule for ionized doping impurities. He suggested that the Fermi level E_F is not able to move up the donor level during deposition because the occupied donor states would be in violation of the "8-N" rule. The auto-compensation doping model has been found unable to explain some experimental results, such as a constant doping efficiency at high dopant levels(Stutzmann, 1986; Stutzmann, Biegelsen and Street, 1987).

From XPS measurements, we have shown in previous sections that 3-fold and

4-fold coordinated Ga can co-exist in the amorphous Si CRN. The fraction of substitutional Ga is closely related to the local Si matrix topological arrangement and to the bond-angle distribution P(θ). This can be seen by the increasing fraction of 4-fold coordinated Ga with increasing annealing temperature. We have shown earlier that P(θ) is determined by the thermal history of the sample. For as-implanted amorphous silicon, the width $\Delta\theta$ of P(θ) is generally very large, and can be decreased through structural relaxation by an anneal. We assume that the dopants have only two possible configurations, sp^2 and sp^3, in an a-Si CRN; this is true for conventional gas-phase GD doped materials. The smaller the $\Delta\theta$ of the Si-Si bond-angle deviations in the tetrahedral Si CRN should give the larger the number of tetrahedral sp^3 dopant, and smaller the number of trigonal sp^2 dopant. In perfect crystalline silicon, $\Delta\theta = 0$. Therefore, Ga atoms are only permitted in substitutional sites (aside from interstitial ones), due to the constraints of periodicity. However, structural relaxation or Si-Si bond-angle ordering of the amorphous silicon CRN does not lead continuously to a crystalline structure. Various experiments, such as differential scanning calorimetry (DSC) (Roorda et al 1989), Raman scattering (Paesler et al 1983, Fortner et al 1988), neutron diffraction (Fortner and Lannin 1989), extended x-ray absorption fine structure (EXAFS) (Paesler et al 1989), and VB-DOS photoemission spectra (section 4.1 of this thesis) have shown that there exists a minimum Si-Si bond-angle deviation $\Delta\theta_{min}$, for which the amorphous silicon CRN is stable , prior to crystallization. This suggests that there should be a corresponding maximum number of subsitutional dopants or a maximum doping efficiency , η_{max}, in this most 'ordered' amorphous silicon. From our XPS measurement, and deductions from electrical measurements by Stutzmann (1986) and Jousse et al.(1987), we found that the solid-phase doping efficiency never exceeds 10 %. We therefore think that the highest doping efficiency (in terms of the fraction of the tetrahedrally bonded dopant) should be around 10 % .

Based on these experimental findings, we propose an alternative way of understanding doping in amorphous silicon, which leads to verifiable predictions of doping efficiency over a wide range of dopant concentrations. The model is based on two main propositions. The first is that when a dopant, say boron, is deposited on a growing a-Si surface, the B atoms may form either sp^2 (B_3^o) or sp^3 (B_4^-) configurations, as shown in Figure 4.9. The relative ratio of the two obviously depends upon the surface Si-Si bond struture, its time of relaxation, and the surface atom mobilities. These are mainly determined by deposition conditions such as substrate temperature and growth rate. We have shown in a previous section that the energy of an sp^2 orbital is lower than that of an sp^3. Therefore, the 3-fold coordinated structure is favored. The tendency of a dopant to occupy a hybrid orbital also depends on its electronegativity relative to that of silicon. According to Bent's rule (Bent 1960. 1961; Huheey, 1978), an sp^3 orbital, which has less s character than that of an sp^2 orbital, is favored when more electronegative substituents such B, P, etc. (see the electronegativities given in Table 4.4) are incorporated into a tetrahedral Si lattice, which we may regard as a "giant silicon molecule". This proposition can be expressed as

$$B_p \rightarrow (1-\alpha)B_3^o + \alpha B_4^- \tag{4.2}$$

where B_p is plasma phase boron and α is the probability of forming a 4-fold configuration.

The second proposition is that when the surface layer is buried into the subsurface and then bulk matrix with the growth of the film, a structural relaxation or Si-Si bond-angle ordering will take place in order to maintain a stable tetrahedral Si CRN. This suggests that bond-angle distortion at a B_3^o site will raise its energy, and it thereby becomes unstable. Heat released during structural relaxation then promotes the unstable B_3^o into a substitutional B_4^-, accompanied by creation of

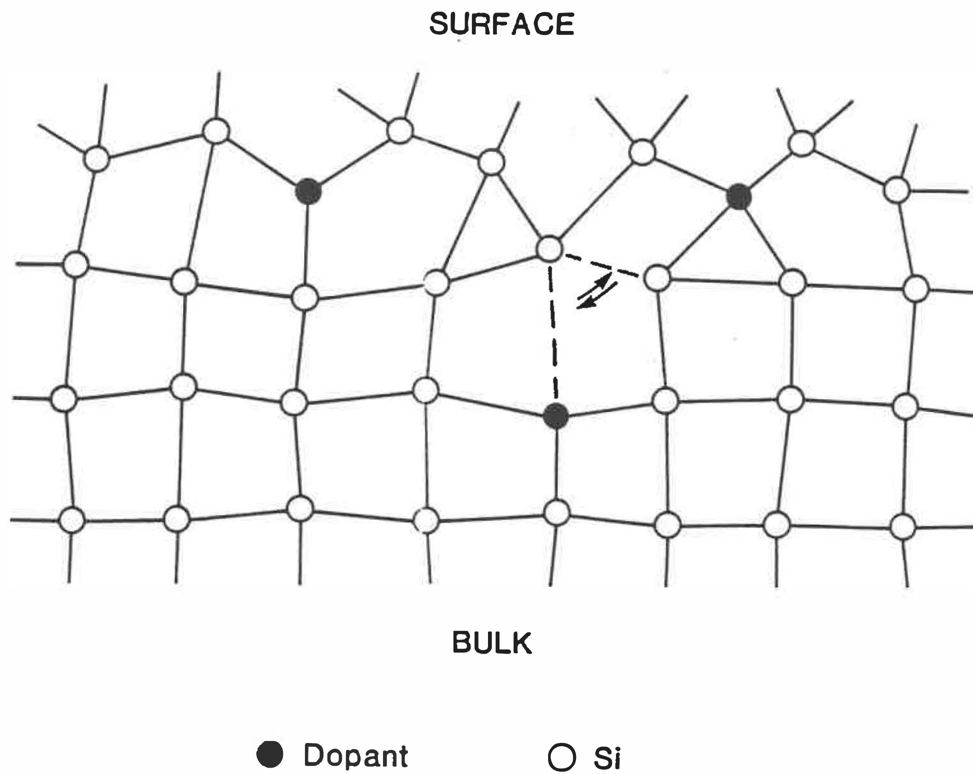

Figure 4.9: A two dimensional a-Si growth model for the incorporation of dopant. At the growing surface, two possible sites for the impurities are shown. At the subsurface, a 3-fold to 4-fold tranition along with the creation of one Si dangling bond is illustrated.

Table 4.4: Elemental Electronegativities of Nontransition Atoms in Tetrahedrally Coordinated Enviroments

Li	Be	B	C	N	O	F
1.00	1.50	2.00	2.50	3.00	3.50	4.00
Na	Mg	Al	Si	P	S	Cl
0.72	0.95	1.18	1.41	1.64	1.87	2.10
(0.9)	(1.2)	(1.5)	(1.8)	(2.1)	(2.5)	(3.0)
Cu	Zn	Ga	Ge	As	Se	Br
0.79	0.91	1.13	1.35	1.57	1.79	2.01
(1.9)	(1.6)	(1.6)	(1.8)	(2.0)	(2.4)	(2.8)
Ag	Cd	In	Sn	Sb	Te	I
0.57	0.83	0.99	1.15	1.31	1.47	1.63
(1.9)	(1.7)	(1.7)	(1.8)	(1.9)	(2.1)	(2.5)
Au	Hg	Tl	Pb	Bi		
0.64	0.79	0.94	1.09	1.24		
(2.4)	(1.9)	(1.8)	(1.8)	(1.9)		

[a] For the first row these have been scaled to agree with Pauling's definition. For other rows Pauling's values are also given (in parentheses)(after Phillips 1973).

one Si dangling bond T_3^+, as shown in Fig. 4.9. This means

$$B_3^o \rightarrow B_4^- + T_3^+ \tag{4.3}$$

However, an increased sustitutional dopant level can increase bond-length and bond-angle variations to the dopant surrounding Si-Si bonds, and consequently increasing Si CRN randomness, which means large Si-Si bond-length deviations. The tetrahedral Ga-Si bonds, for example, are responsible for the Si-Si bond-length and bond-angle deviations in crystalline silicon (see details in section 4.7). The tetrahedral As–Si–Si bond angle in crystalline silicon, has also been found to produce about a 3° deviation from the ideal Si–Si–Si bond-angle, as indicated by EXAFS measurements(Erbil et al 1986). So the B_3^o to B_4^- transition is maintained at a thermal equilibrium which is controlled by the a-Si CRN topological arrangement or bond-angle distribution function $P(\theta)$. Then, the above equation can be written as

$$B_3^o = B_4^- + T_3^+ \tag{4.4}$$

From the law of mass action, we have

$$N_3 = Const.N_4^2 \tag{4.5}$$

where N_4 is the substitutional B concentration promoted from trigonal B_3^o, along with same amount of silicon T_3^+ defect created. The solid-phase doping efficiency η_{sol} is then given by

$$\eta_{sol} = (\alpha N_o + N_4)/N_o = \alpha + const.N_3^{1/2}/N_o \tag{4.6}$$

where N_o is the total solid-phase dopant concentration. As the doping efficiency is generally very low, we can make the aproximation $N_o \approx N_3$. We know that α is only related to the dopant's chemical properties and deposition conditions. Therefore η_{sol} can be expressed as

$$\eta_{sol} = \alpha(Z, \kappa) + \beta(Z, P(\theta)) \cdot N_o^{-1/2} \tag{4.7}$$

where $\alpha(Z, \kappa)$ and $\beta(Z, P(\theta))$ are constants related to the doping element Z (group III and V elements), deposition parameter κ, and the Si CRN bond-angle distribution function, P(θ).

The above equation indicates that the doping efficiency of all group III and V dopants, will be dominated by the square-root term at low dopant concentrations. A constant value is expected at higher dopant concentrations. The experimental variations of doping efficiency with dopant concentrations are shown in Figure 4.10 (Stutzmann, 1986). The results indicate that η_{sol} has a square-root relation for B and P in a-Si:H and P in a-Ge:H. and a constant value for As in a-Si:H and B in a-Ge:H over the dopant range measured. This is in excellent agreement with the predictions of our doping model.

As we have discussed above. the B_3^o to B_4^- transition is related to adjustments in the bond-angle distribution. P(θ). Therefore a decrease in the width, $\Delta\theta$, of P(θ) will lead to an increase in doping efficiency. It has been reported that a-Si:H films deposited at low temperature possess larger $\Delta\theta$ than those deposited at high temperature, and $\Delta\theta$ can be reduced by post-annealing (Beeman 1985; Paesler et al 1983; Tsu et al 1984). Fiorini et al (1987) have found a significant increase in doping efficiency by annealing low temperature deposited a-Si:H. This, in our view, is due to an increasing β(Z.P(θ)) induced by annealing, which narrows the bond-angle distribution function P(θ) of the Si CRN.

Eq.(4.4) indicates that creation of a 4-fold coordinated acceptor from a 3-fold coordinated boron is accompanied by the creation of one defect. Such a dopant-defect pair formation or auto-compensation mechanism was first proposed by Street (1982), but based on a very different physical principle. That is, Street suggested that the transition between B_3^o and B_4^- is controlled by the carrier Fermi level E_F. However, we believe that the fraction of substitutional dopant is

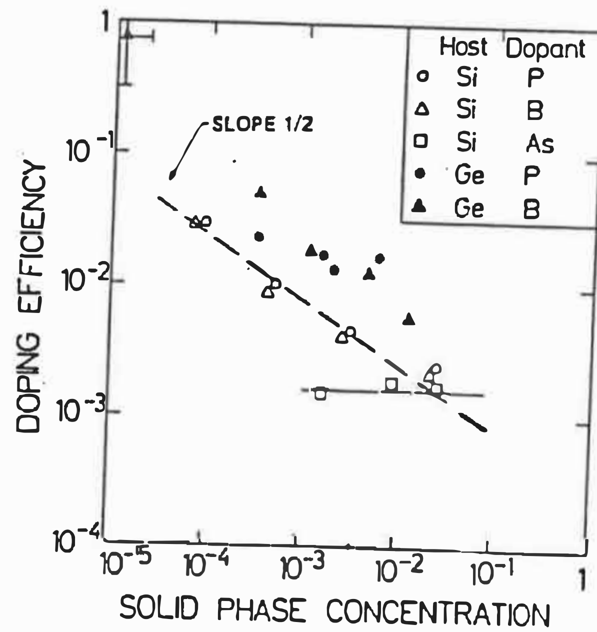

Figure 4.10: Doping efficiency for P. As and B in glow discharge deposited a-Si:H and a-Ge:H as a function of the dopant concentration in the solid-phase(from Stutzmann (1986)).

determined by the Si amorphous CRN bond-angle distribution function P(θ).

4.6 Supersaturated Substitutional Ga in Crystalline Silicon Studied by Si 2p Core Level Spectra

In Figure 4.11, we show Si 2p core level spectra recorded on ion-implanted c-Si samples annealed at temperatures from 500 to 900 °C. Binding Energies are aligned at 99.6 eV. The Si 2p spin-orbit doublet with an energy separation of 0.60 eV and intensity ratio of 1:2 is well described by a mixed Lorentzian (0.8) and Gaussian (0.2) convolution function. The FWHM of the convolution function ranges from 0.8 to 0.7 eV, depending upon the Ga-induced strains. The strains and static charge fluctuations in the c-Si lattice will be discussed in detail in the next section.

Two Si 2p doublets, one at 99.6 eV and the other, shifted by 0.6 eV to 99.0 eV, are deconvoluted for samples annealed at temperatures ranging from 500 to 800 °C, as shown in the figure. Only one doublet, at 99.6 eV is found to best fit the experiment data for samples annealed at 900 °C. The peak at 99.6 eV binding energy is from Si atoms which are normally bonded to 4 other Si atoms in a c-Si lattice. The peak with a chemical shift of 0.6 eV to low binding energy is interpreted as being due to the Si which is bonded to three other Si, and to one tetrahedrally coordinated Ga. This is based on the following: First, the good crystalline structure of the solid-phase regrown silicon lattice makes other Ga bonding formulas such as the trigonal sp^2 hybrid, very unlikely. Second, we can exclude the possibility that the peak is due to $SiGa_2$, $SiGa_3$ or $SiGa_4$ clusters , as shown in Figure 4.12, because the probability of those arrangements is very small in comparison to the isolated Ga-in-Si structure of Fig. 4.11(d),

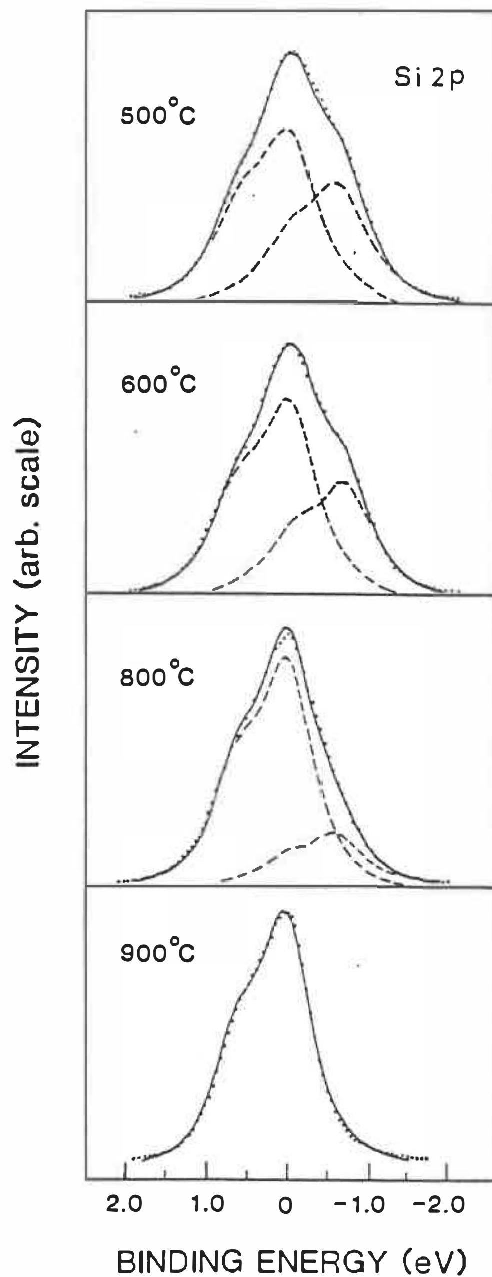

Figure 4.11: Si2p core level spectra recorded on Ga^+-implanted c-Si samples after being annealed at various temperatures. The data points are shown as dots. The dashed curves show the bulk and chemically shifted peaks and the solid curve is the sum of the two components. Intensities are shown on an arbitary scale and binding energies are aligned to 99.6 eV.

and only one chemically shifted peak is observed. A quantum chemical ab-initio calculation of the isolated substitutional Ga-in-Si structure model indicates that this Ga configuration should produce a Si 2p core level shift of 0.6 - 0.7 eV toward lower binding energy(Selmani 1989), in excellent agreement with the experimental result.

No indication of a Si 2p core level shift has been found for samples annealed at low temperature($\leq$400 °C). From Ga 3d core level measurements on these samples, we have shown that only a small fraction of gallium is in the tetrahedral sp^3 state, the majority being in either a 3-fold coordinated trigonal sp^2 hybrid or an interstitial elementary state Ga^o. The broadened Si 2p peak makes the Si-Ga bond-induced shift too small to be resolved. The correlation between Si 2p core level FWHM and valence shell static charge fluctuations will be the subject of a comprehensive discussion in the next session.

The tetrahedrally coordinated gallium concentration is determined by measuring the intensity ratio of Si2p(-Ga)/Si2p, where Si2p(-Ga) and Si2p mean the shifted and total spectra intensity, respectively(the first row of Table 4.5), and dividing by 4 (4 Si-Ga bonds for each Ga atom). The results are shown in the second row of Table 4.5, where we can see that 10 at.% substitutional Ga has been obtained after annealing at 500 °C. We also see that the Ga concentration decreases with increasing annealing temperatures, to a value too low to be detected by XPS after an anneal at 900 °C. We explain this as due to increased silicon lattice structural relaxation at increased annealing temperature. This releases the Si-Ga bond-induced strains: that is, it reduces the Ga induced bond-angle and -length deviations of the surrounding Si-Si bonds. This process is accompanied by an evolution of heat. Consequently, the substitutional Ga atoms are excluded from the lattice and diffuse. This hypothesis is strongly supported by the observation of an activation energy of 0.2($\pm$0.1) eV in an Arhenius plot of the Ga concentration and annealing temperature, as shown in Fig. 4.13. A comparable

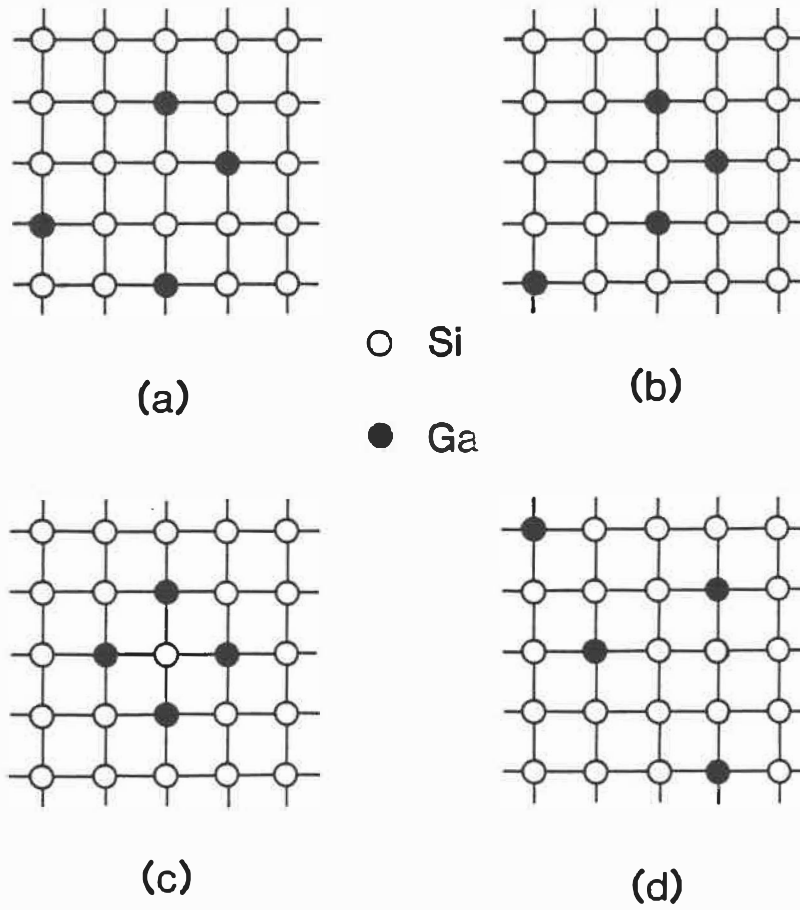

Figure 4.12: A two dimentional model of four different possible Ga-in-Si configurations; cases (a), (b) and (c) correspond $SiGa_2$, $SiGa_3$ and $SiGa_4$ clusters, respectively; case (d) is the isolated Ga-in-Si structure.

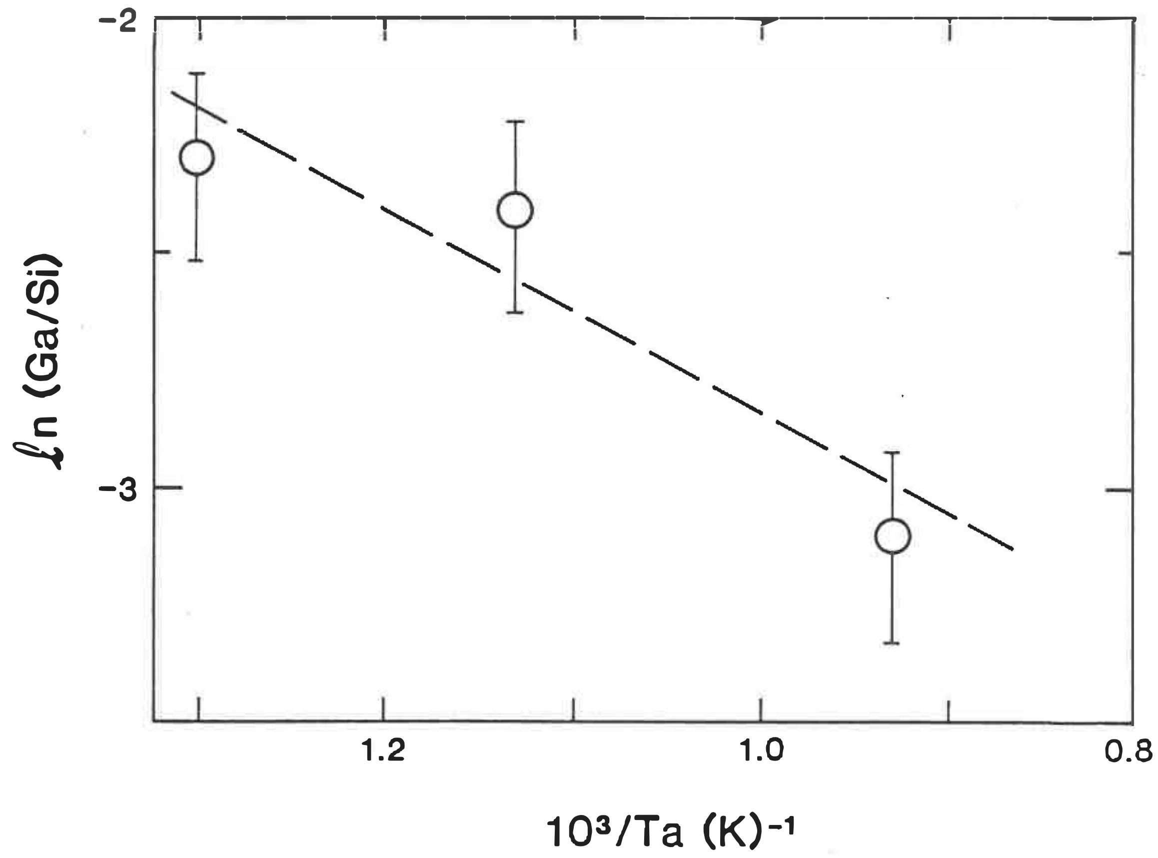

Figure 4.13: Arrhenius plot of the substitutional gallium and annealing temperature.

activation energy of 0.16 eV has been reported by Fortner and Lannin (1988) in the exothermic bond-angle ordering process, by annealing Ar^+-implanted Si and Ge. The same physical mechanism, as we have discussed in section 4.4, is responsible for the promotion of trigonal and tetrahedral Ga from the elementary as-implanted state at low annealing temperatures.

Several reseach groups have reported (Matsuo et al 1987; Harrison et al 1987; Lin et al 1988) that the hole-carrier levels of Ga^+-implanted Si, at doses over the Ga solid solubility limit in Si, decrease with increasing annealing temperatures higher than 600 °C. This "abnormal" activation behaviour of Ga-in-Si, however, can be easily understood from our data. That is, strains produced by the supersaturated substitutional Ga are released at increased annealing temperatures, excluded the Ga from the substitutional sites, and consequently there is a reduction of hole-carrier levels.

The valence-band density-of-state (VB-DOS) spectra of these samples recorded at the same time were shown in Fig. 4.3. The valence band maxima (VBM) were determined in the usual way (Ley 1984), through the extrapolation of the steepest descent of the leading edge of the VB-DOS. We measured the binding energy difference between the Si $2p_{3/2}$ core level and the VBM, and found it changed significantly, while the width of the VB remained unchanged.

It is interesting that the binding energies of Si 2p levels of those samples vary randomly less than 0.2 eV, in reference to the Fermi level of the spectrometer. This is mainly due to the statistical fluctuations and sample surface charge or contamination level variations.

The shift towards vacuum level of the VBM, ΔE_{VBM}, relative to a virgin silicon sample, is given in Table 4.5. This shift cannot be due to surface band bending, as band bending will move both the core level and VB-DOS in the same direction. We attribute the shift on samples annealed at 300 °C to the amorphous nature of the damaged layer. The same shift has been found on as-implanted Si samples and

Table 4.5: XPS Data for Ga^+-Implanted c-Si as a Function of RTA Temperature.

RTA Temperature (°C)	300	400	500	600	800	900	Virgin Si(100) (0.003-0.007Ωcm)
Si(-Ga)/Si			0.41	0.36	0.18	0.0	
Ga/Si (at.%)			10	9	4.5	0	
ΔE_{VBM} (eV)	0.4	0.1	0.7	0.6	0.1	0.0	0(reference)
LEED Pattern observed	no	no	yes	yes	yes	yes	

also on sputtered a-Si (Ley 1984). The recession of the VBM for samples annealed at 400 ^oC again suggests that the Si lattice has been partially reconstructed, as we have discussed in section 4.2. However, ΔE_{VBM} increases drastically, as does the substitutional Ga concentration, on samples annealed at temperatuires higher than 500 ^oC (see Table 4.5). We believe these shifts to be due to Si-Ga bonding states, which induce a shift of the Si valence electrons to lower binding energy. In comparison, Si-H bonds are found, by both photoemission spectroscopy and various band calculations (Ley 1984), to produce a VBM recession, consequently enlarging the energy band gap as the conduction band minimum (CBM) remained unaffected by the Si-H anti-bonding states. Unforturnately, based on current experiments, we are unable to determine whether the CBM is changed by Si-Ga anti-bonding states. There are no corresponding energy band calculations available at the time of writing. However, other experimental studies on Al, which also has a lower electronegativity than that of Si, show that Al can narrow the a-Si:H energy band gap at concentrations higher than 3 at.% (Thompson and Reinhard 1980; Lu 1986; Liu and Lu 1986; Saito et al 1989). This suggests that the c-Si energy band-gap might be narrowed by the supersaturated subsitutional Ga.

The surface crystallinity of the implanted and annealed samples was examined by LEED measurements. The results are given in table 4.5. The observation of LEED patterns on Ga^+-implanted c-Si after annealing at temperatures $\geq$ 500 ^oC, suggests that SPE regrowth of the damaged layer has been extended to the surface, in good agreement with VB-DOS measurements.

4.7 Static Charge Fluctuations in Si

We have shown in previous section that the FWHM of the Si 2p core levels decreases with increasing annealing temperatures. This is shown in Table 4.6.

As the data were collected under identical instrument conditions, the FWHM contributed by X-ray source and electron energy analyser should be the same. So the symmetric broadening of Si 2p core levels in ion-implanted and annealed samples, measured under identical instrument conditions, is due to the static charge fluctuations in the valence shell electron distributions, as it is in sputtered a-Si (Ley 1982) and silicon oxides (Grunthaner 1987). The valence shell electron fluctuations, which means either electron rich or lean in compared to ideal charge distributions in the Si valence shell, will cause the core levels to shift on both sides of the ideal peak position. The broad peak observed, therefore, is actually the sum of all these shifted and unshifted peaks. We can write such interpretation as

$$f(E,\zeta) = B \cdot f(E,\zeta_o) + \sum_{E_i \neq E} C_i \cdot f(E_i, \zeta_o) \tag{4.8}$$

where $f(E,\zeta)$ is the convolution function with binding energy E and FWHM ζ; ζ_o is the FWHM measured on virgin c-Si under identical instrument conditions, i.e., 0.7 eV. E_i is the binding energy of those silicon atoms with valence charge deviation of Δq_i. B and C_i are the corresponding spectra intensities. As an approximation, we may rewrite the above equation as

$$f(E,\zeta) \approx B \cdot f(E,\zeta_o) + C \cdot f(E + \Delta E_{rms}, \zeta_o) + C \cdot f(E - \Delta E_{rms}, \zeta_o) \tag{4.9}$$

where B, C and ΔE_{rms} can be determined using a least-square fitting of the sum of right-hand terms to the left-hand term, for a given ζ and E. The goodness of fit obviously depends on the value of ζ. The physical meaning of the above equation is that the overall effects of these Si atoms with valence charge fluctuation of Δq_i and with core level chemical shift of $(E - E_i)$ are summarized as Si atoms with a percentage of 2C/B, and with a mean charge fluctuation of Δq_{rms}, which causes the same core level shift of ΔE_{rms}. The two terms with opposite signs of chemical shifts represent the observed symmetric broadening of the 2p core levels.

It has been reported (Grunthaner et al 1979) that the loss or gain of one electron in the Si valence shell will lead to a 2p core level shift of 2.2 eV. We know that the chemical shift is related to charge transfer through eq.(2.10), Therefore, the mean static charge fluctuations Δq_{rms} on each Si atom can be estimated by 2C$\cdot\Delta E_{rms}$/2.2B. The calculated Δq_{rms} and corresponding ζ are given in Table 4.6.

From the table we see that a large FWHM value of 1.0 eV for samples annealed at or below 400 °C, yields a static charge fluctuations of 0.11 electrons units rms. The same amount of Δq_{rms} in sputtered a-Si was reported by Ley et al (1982) using a different method of estimation. A value for Δq_{rms} of 0.2 electrons on atoms of an amorphous silicon cluster was also calculated by Guttman et al (1980). This indicates that static charge fluctuations in these samples are due to the unreconstructed Ga^{+}-ion amorphized Si lattice, in good agreement with VB-DOS and LEED measurement results.

For samples annealed at or above 500 °C, a significant amount of Ga has been promoted to substitutional sites in a well reconstructed Si lattice. The static charge fluctuations in these samples is explained as largely being due to substitutional Ga. This is understandable. As the Si-Ga bond-length (2.398 Å) is larger than that of Si-Si bond (2.346 Å) (Phillips 1973) in pure silicon, the substitutional Ga will induce bond-angle and bond-length deviations in the first. second, or further neighbor Si-Si bonds. Consequently, the bond-angle and bond-length deviations will lead to Si valence shell charge distribution fluctuations as indicated by the calculation (Guttman et al 1980).

Table 4.6: Calculated Static Charge Fluctuations in Ga^{+}-Implanted Si as a Function of Annealing Temperature.

RTA Temperature (°C)	300	400	500	600	800	900	Virgin Si(100) (0.003-0.007Ωcm)
FWHM (eV)	1.00	1.00	0.80	0.75	0.72	0.70	0.70
Ga/Si (at.%)			10	9	4.5	0	
$<\Delta q>$ ($\|e\|$)	0.11	0.11	0.04	0.02	0.003		

Chapter 5

Conclusion

In this thesis, we have demonstrated feasibility of shallow p^+ doping in silicon by LMIG Ga^+ ion implantation. Supersaturated Ga-in-Si was obtained by 4 keV Ga^+ implantation and rapid thermal annealing. XPS has been successfully used for the first time to study the physical chemistry of Ga-in-Si, and Si lattice structural relaxation and crystallization processes.

Studies of valence band density of states (VB-DOS) indicate that c-Si lattice has been amorphized by 4 keV Ga^+ ions at a dose of 15 at.%. This is seen by the observation that the two 3s-like bands of states have merged into a hump, which is attributed to an averaging of a variety of local Si bonding topologies. The two 3s-like bands of states were found to be merged after being annealed at temperatures $\leq 300°C$, and to become distinct for samples annealed at temperatures $\geq 350°C$. Distinct c-Si VB-DOS structural features were observed on samples annealed at or above 500 °C. LEED studies show that RTA annealing-induced solid-phase epitaxial (SPE) regrowth extended to the surfaces on samples annealed at temperatures $\geq 500°C$.

We found that the valence band electron density of states had been significantly modified by the presence of Ga atoms. The observed "extra" density of states at an energy of about 10 eV (peak III region) is interpreted as due to the

contribution of the two 4s valence electrons of the unactivated elementary Ga atoms. With increasing annealing temperature, there is an increasing extent of Ga atoms hybridizing with Si atoms. and, consequently, a decreasing density of states in peak-III region, as observed.

From Ga 3d core level measurements, we found that the majority of as-implanted Ga is in the elementary state Ga° along with very small amount of 2-fold coordinated Ga bonded to the damaged Si lattice. The 2-fold coordinated Ga is found an unstable state and disappears on annealing. On the other hand, the low temperature annealing ($\leq 500^{\circ}C$) activated Ga atoms are shown to be in either an sp^2 or an sp^3 hybrid. The concentration of 3-fold coordinated Ga is twice as high as that of the substitutional Ga. which is attributed to the slight difference in their hybrid orbital energies. Further studies show that the heat, H_{SR}, released by the Si structural relaxation or bond-angle ordering(prior to crystallization), is the prime energy source for the activation of the dopant. An activation energy of 0.14 eV in the thermal process of Ga valence electron hybridization is deduced for both trigonal sp^2 and tetrahedral sp^3 states. The fraction of substitutional Ga or the doping efficiency in amorphous silicon is measured and found to vary from 5 to 10 %. We suggest that the fraction of the substitutional dopants is closely related to the amorphous silicon CRN bond-angle distribution function $P(\theta)$.

A $P(\theta)$ controlled dopant-defect auto-compensation doping mechanism in amorphous silicon is proposed. The model predicts that the doping efficiency η_{sol} has a square-root relation to the dopant concentration N_o at low doping level, and a constant value at higher levels. We also suggest that there should be a maximum η_{sol} of about 10 %, which corresponds to $\Delta\theta_{min}$, the minimum width of $P(\theta)$ capable of maintaining a-Si CRN in a stable state prior to crystallization.

From Si 2p core level measurements, we have observed a tetrahedral Si-Ga bonding state induced peak which has a chemical shift of 0.6 eV to the lower binding energy. The Ga, as high as 10 at. % , was found in isolated substitutional

sites after an anneal at 500 °C for 5s. With the release of strains due to increased Si lattice structural relaxations at higher annealing temperatures, the Ga leaves the substitutional sites. The Si-Ga bonds are shown to be responsible for the VBM shift towards the vacuum level.

The FWHM of Si 2p core level electrons is found to decrease with increasing annealing temperature. A large FWHM of 1.0 eV for samples annealed at low temperature($\leq$ 400°C) is attributed to Si-Si bond-length and bond-angle variations and consequent static charge fluctuations Δq_{rms} in the unreconstructed amorphous silicon CRN. For a well reconstructed Si lattice after being annealed at or above 500 °C, however, Δq_{rms} is shown to be caused by Si-Ga bond-induced strains. We have estimated that Δq_{rms} in amorphous silicon is 0.11 electrons, and, in c-Si, it ranges from 0.04 to 0.003 electrons, depending upon the Si-Ga bond densities.

I have demonstrated in this thesis that photoelectron spectroscopy can be used to study the bulk properties of silicon. In what follows I will list some of the interesting problems that can be studied with XPS; (1) The structural relaxations in Si^{+}-implanted and amorphised silicon samples. (2) The structural relaxations in low temperature deposited and annealed amorphous silicon samples. (3) The electrical and optical properties of the highly degenerated c-Si. (4) Fabrication of shallow p^{+}+-n junction and related devices. (5) Studying of other p-type and n-type dopant properties in both crystalline and amorphous silicons.

Bibliography

[1] Appelbaum, J.A., Hamann, D.R. (1976) *Rev. Mod. Phys.*,**48**, 479; (1978),*Crit. Rev. Sol. State Sci.*,**6**, 357.

[2] Beeman, D., Tsu, R., and Thorpe, M.F.(1985) *Phys. Rev.* **B**, **32**, 874.

[3] Bent, H.A.(1960) *J. Chem. Phys.*,**33**, 1258; (1961) *Chem. Rev.*,**61**, 275.

[4] Bose, S.K., Winer, K., and Anderson, O.K.(1988) *Phys. Rev.* **B**,**37**, 6262.

[5] Brebner, J.L. et al(1985) *Can. J. Phys.*, **63**, 786.

[6] Briggs, D., and Seah, M.P.(1983) in *Practical Surface Analysis by Auger and X-ray Photoelectron Spectroscopy*, edited by D. Briggs and M.P. Seah, (John Wiley & Sons, New York), p.511.

[7] Bringan, R.D., Olmstead, M.A., Uhrberg, R.I.G., and Bachrach, R.Z.(1987) *Phys. Rev.* **B**, **36**, 9569.

[8] Burrows, V.A., Chabal, Y.J., Higashi, G.S., Raghavachari, K., and Christman, S.B. (1988) *Appl. Phys. Lett.*,, **53**, 998.

[9] Cardona, M., and Ley, L.(1978) in *Photoemission in Solids I*, edited by M. Cardona and L. Ley, (Springer-Verlag, New York), p.1.

[10] Chabal, Y.J., Higashi, G.S., and Raghavachari, K.(1989) *J. Vac. Sci. Technol.* **A**, May(in press).

[11] Chen P.W.(1985) in *Handbook of University Physics*, edited by Chen P.W. (Xinhua, Shandong), p.433.

[12] Ching, W.Y., Ling, C.C., and Huber, D.L.(1976) *Phys. Rev.* **B**, **14**, 620.

[13] Ching, W.Y., Ling, C.C., and Guttmann, L.(1977) *Phys. Rev.* **B**, **16**, 5488.

[14] Donovan, E.P., Spaepen, F., Turnbull, D., Poate, J.M., and Jacobson, D.C.(1984) *J. Appl. Phys.*, **57**, 1795.

[15] Eastman, D.E., Heimann, P., Himpsel, F.J., Reihl, B., Zehner, D.M., and White, C.W.(1981) *Phys. Rev.* **B**, **24**, 3647.

[16] Elliott, S.R.(1983) *Physics of Amorphous Materials*, Longman, London, p.94.

[17] Fenner, D.B.,Biegelsen, D.K., Bringans , R.D., and Krusor, B.S. (1989a) *Materials Research Society Symposium Proceedings*, San Diego, April 24-29 (in press).

[18] Fenner, D.B., Biegelsen, D.K.. Bringans, R.D. (1989b) *J. Appl. Phys.*, July (in press).

[19] Fiorini, P., Haller, I., Nocera, J.J., Cohen, S.A., and Brodsky, M.H.(1987) *J. Appl. Phys.*, **62**, 1425.

[20] Forstmann, F. (1977) in *Photoemission from Surfaces*, edited by B. Feuerbacher, B. Fitton, R.F. Willis(Wiley, New York), Chap.8.

[21] Fortner, J. and Lannin. J.S.(1988) *Phys. Rev.* **B**, **37**, 10154.

[22] Fortner, J. and Lannin, J.S.(1989) *Phys. Rev.* **B**, **39**, 5527.

[23] Fritzche, H.(1984) in *Semiconductors and Semimetals*, edited by J.I. Pankove, (Academic Press, New York), vol.21C, p.309.

[24] Ghosh. P.K.(1983) *Introduction to Photoelectron Spectroscopy*, John Wiley and Sons, New York, p.161.

[25] Graf, D., Grundner, M., and Schulz, R.(1989) *J. Vac. Sci. Technol.* **A**, May(in press).

[26] Grunthaner, F.J., Grunthaner, P.J., Vasquez, R.P., Lewis, B.F., Maserjian, J., and Madhukar, A. (1979) *Phys. Rev. Lett.*, **43**, 1683.

[27] Grunthaner, P.J., Hecht, M.H., Grunthaner, F.J., and Johnson, N.M. (1987) *J. Appl. Phys.*, **61**, 629.

[28] Guttman, L., Ching, W.Y., and Rath, J. (1980) *Phys. Rev. Lett.*, **44**, 1513.

[29] Harrison, H.B., Iyer, S.S.. Sai-Halasz, G.A., and Cohen, S.A. (1987) *Appl. Phys. Lett.*, **51**, 992.

[30] Harrison, W.A.(1981) *Phys. Rev.* **B**, **24**, 5835.

[31] Huheey, J.E.(1978) *Inorganic Chemistry*, 2nd ed., (Harper and Row, New York), p.159.

[32] Jacobsen, D.C., Poate, J.M., Eaglesham, D.J., and Chen, H.S. (1989) *Materials Research Society Symposium Proceedings*, San Diego, April 24-29 (in press).

[33] Joannopoulos, J. and Cohen, M.H.(1976) *Solid State Phys.* **31**, edited by H. Ehrenreich, F. Seitz, and D. Turnbull, (Academic , New York).p.71.

[34] Jousse, D., Bruyere, J.C., Bustarret, E., and Deneuville, A. (1987) *Phil. Mag. Lett.*, **55**, 41.

[35] Knights, J.C., Hayes, T.M., and Mikkelsen, Jr., J.C.(1977) *Phys. Rev. Lett.*, **39**, 712.

[36] Kazahaya, T., and Hirose, M.(1986) *Japan. J. Appl. Phys.*, **25**, L75.

[37] Lang, B., and Taofik, A.(1986) *Appl. Phys.* **A**, **39**, 95.

[38] Lau, W.M.(1989), private communication.

[39] Ley, L., Kowalczyk, S.P., Pollak, R.A., and Shirley, D.A.(1972). *Phys. Rev. Lett.*, **29**, 1088.

[40] Ley, L., Reichardt, J., and Johnson, R.L. (1982) *Phys. Rev. Lett.*, **49**, 1664.

[41] Ley, L. (1984a) in *The Physics of Hydrogenated Amorphous Silicon II*, edited by J.D. Joannopoulos and G. Lucovsky, (Springer-Verlag, New York), p.61 and references therein.

[42] Ley, L.(1984b) In *Semiconductors and Semimetals*, edited by J.I. Pankove, (Academic Press, New York), vol.21B, p385.

[43] Lin, C.M., Steckl, A.J., and Chow, T.P. (1988) *Appl. Phys. Lett.*, **52**, 2049.

[44] Liu, J.M. and Lu, Z.H. (1986) *Proc. of 2nd Intern. Photovolt. Sci. and Eng. Conf.*, Beijing, p.557.

[45] Lu, Z.H. (1986) *M.S. Thesis*, Yunnan University.

[46] Lu, Z.H., Lagarde, C., Currie, J., and Yelon, A. unpublished.

[47] Lu, Z.H., Sacher, E., and Yelon, A.(1988) *Phil. Mag.*, **58**, 385.

[48] Lu, Z.H., Sacher, E., Selmani, A., and Yelon, A.(1989a) *Appl. Phys. Lett.*, **54**, 2665.

[49] Lu, Z.H., Largade, C., Sacher, E., Currie, J., and Yelon, A. (1989b) *J. Vac. Sci. Technol.* **A**, **7**, 646.

[50] Lu, Z.H., Azelmad, A., Trudeau, Y., and Yelon, A.(1989c) *Appl. Phys. Lett.*, **55**, 846.

[51] Margaritondo, G. and Weaver, J. (1985) in *Solid State Physics: Surfaces*, edited by L. Park and M.G. Lagally, (Academic Press, New York), p.131.

[52] Matsuo, J., Kato, I., Horie, H., Nakayama, N., and Ishikawa, H. (1987) *Appl. Phys. Lett.*, **51**, 2037.

[53] Michel, E., Kastl, R.H., Mader, S.R., Masters, B.J. and Gardener, J.A. (1984) *Appl. Phys. Lett.*, **44**, 404.

[54] Mott, N.F.(1967) *Adv. Phys.*, **16**, 49.

[55] Nakazawa, M., Nishioka, Y., Sekiyama, H., and Kawase, S.(1989) *J. Appl. Phys.*, May(in press).

[56] Ortenburger, I.R., Rudge, W.E., and Herman, F.(1972). *J. Non-Cryst. Solids*, **8-10**, 653.

[57] Paesler, M.A., Sayer, D.E., Tsu, R., and Hermandez, J.G.(1983). *Phys. Rev.* **B**, **28**, 4550.

[58] Pankove, J.I.(1984) *Semiconductors and Semimetals*, edited by J.I. Pankove (Academic, New York), vol21A-C. In these four volumes, both the physical and technical aspects of hydrogenated amorphous silicon were critically reviewed by numerical experts in this field.

[59] Pauling, L. (1967) *The Nature of the Chemical Bond*. (Cornell Univ. Press, New York).

[60] Phillips, J.C.(1973) *Bonds and Bands in Semiconductors*, (Academic Press, New York & London), p.54.

[61] Reimer, J.A., and Duncan, T.M.(1983) *Phys. Rev.* **B**, **27**, 4895.

[62] Robertson, J.(1983) *Phys. Rev.* **B**, **28**, 4666.

[63] Roorda, S., Doorn, S., Sinke, W.C., Scholte, P.M.L.O., and van Loenen, E. (1989) *Phys. Rev. Lett.*, **62**, 1880.

[64] Sacher, E., Klemberg-Sapieha, J., Wertheimer, M.R., Schreiber, H.P. and Groleau, R.(1984) *Phil. Mag.*, **B**, **49**, L47.

[65] Saito, N., Tomioka, Y., Yamaguchi, T., and Kawamura, K.(1989) *Phil. Mag. Lett.*, **59**, 43.

[66] Selmani, A.(1989) to be published.

[67] Shirley, D.A. (1972) *Phys. Rev.* **B**, **5**, 4709.

[68] Siegbahn, K., Nordling, C., Fahlman, A., Nordberg, K., Hamrin, K., Hedman, J., Johansson, G., Bergmark, T., Karlsson, S.E., Lindgren, I., and Lindberg, B. (1967) *ESCA; Atomic, Molecular and Solid State Structure By Means of Electron Spectroscopy*, (Almqvist and Wiksells, Uppsala), p.71.

[69] Spear, W.E. and LeComber, P.G.(1975) *Solid State Commun.*, **17**, 1193.

[70] Spicer, W.E. (1958) *Phys. Rev.*, **112**, 114.

[71] Stern, Z.A., Bouldin, C.E., Von Roedern, B., and Azoulay, J. (1983) *Phys. Rev.* **B**, **27**, 6557.

[72] Street, R.A.(1982) *Phys. Rev. Lett.*, **49**, 1187.

[73] Stutzmann, M.(1986) *Phil. Mag.* **B**, **53**. L15.

[74] Stutzmann, M., Biegelsen, D.K., and Street, R.A.(1987) *Phys. Rev.* **B**, **35**, 5666.

[75] Swartzentruber, B.S., Mo, Y.W., Webb, M.B., and Lagally, M.G. (1989) *J. Vac. Sci. Technol.* **A**, (in press).

[76] Thompson, M.G., and Reinhard, D.K. (1980) *J. Non-Cryst. Solids*, **37**, 325.

[77] Tsu, R., Hermandez, J.G., and Pollak, F.H.(1984) *J. Non-Crys. Solids*, **66**, 109.

[78] Vasquez, R.P., Madhukar, A. and Tanguay, A.R.(1985) *J. Appl. Phys.*, **58**, 2337.

[79] Wach, W. and Wittmaack, K.(1983) *Phys. Rev.*, **B, 27**, 3528.

[80] Weaire, D. and Thorpe, M.F.(1971) *Phys. Rev.* **B**, **4**, 2548, 3517.

[81] Wertheim, G.K. (1978) in *Electron and Ion Spectroscopy of Solids*, edited by L. Fiermans, J. Vennik and W. Dekeyser, (Plenum Press, New York), p.192.

[82] Winer, K.(1987) *Phys. Rev.* **B**, **35**, 2366.

[83] Ziegler, J.F., Biersack, J.P. and Littmark, U.(1985) *The Stopping and Range of Ions in Solids*, Pergamon Press, New York.

ÉCOLE POLYTECHNIQUE DE MONTRÉAL
3 9334 00291696 1